General Disclaimer

One or more of the Following Statements may affect this Document

- This document has been reproduced from the best copy furnished by the organizational source. It is being released in the interest of making available as much information as possible.

- This document may contain data, which exceeds the sheet parameters. It was furnished in this condition by the organizational source and is the best copy available.

- This document may contain tone-on-tone or color graphs, charts and/or pictures, which have been reproduced in black and white.

- This document is paginated as submitted by the original source.

- Portions of this document are not fully legible due to the historical nature of some of the material. However, it is the best reproduction available from the original submission.

Produced by the NASA Center for Aerospace Information (CASI)

Department of AERONAUTICS and ASTRONAUTICS
STANFORD UNIVERSITY

(NASA-CR-174138) THE 1984 NASA/ASEE SUMMER FACULTY FELLOWSHIP PROGRAM Final Report (Stanford Univ.) 90 p HC A05/MF A01 N85-13663
CSCL 05I Unclas
G3/80 24534

1984

TECHNICAL REPORT

NASA/ASEE SUMMER FACULTY FELLOWSHIP RESEARCH PROGRAM

STANFORD-AMES-DRYDEN FRF

DEC 1984
RECEIVED
NASA STI FACILITY
ACCESS DEPT.

SEPTEMBER 1984

1ST-YEAR FELLOWS

Extraction of topographic networks from digital elevation data

Lawrence E. Band

Hunter College
City University of New York
Assistant Professor of Geology and Geography

Many projects in hydrology, ecology and related disciplines require the extraction and organization of environmental data bases by watersheds. The Extraterrestrial Research Division at NASA-Ames is currently engaged in research assessing forest productivity and associated nitrogen flux in a number of conifer ecosystems. The work is partially in cooperation with the National Park Service as a base line study of acid precipitation in the Sierra Nevada. As such, the study involves the extraction and integration of a number of data planes describing the terrain, soils, lithology, vegetation cover and structure, and microclimate of the region.

My work this summer has involved the development of automated techniques to extract topographic networks (stream canyons and ridge lines) for use as a landscape skeleton to organize and integrate these data sets into an efficient geographical information system. The techniques are applicable to a wide range of environmental problems outside of the present application. The software is written in both Fortran and C, and should be portable to a number of different computer environments with minimal modification. The data input consists of a standard raster elevation file such as the digital elevation model (DEM) produced by the USGS or the digital terrain model (DTM) produced by the DMA. Output consists of the set of connected drainage divides and stream lines such that the drainage divides completely partition the image plane into drainage polygons, which are uniquely associated to a link in the stream network structure.

The topographic networks are first unambiguously defined in a geomorphic framework and then processes in a multi-step procedure which first nominates potential stream and ridge lines, and then successively grows and refines the features into geomorphically reasonable, connected graph structures representing fully complementary drainage channel and drainage divide networks (figure 1). The stream network is a directed tree graph, rooted at an outlet node. Its node set intersects the node set of the drainage divide graph at all stream junctions. The specific topologic properties and relations between the two graph structures allows the construction of a powerful set of topological and

geometrical manipulations of the graphs and of the data sets they organize.

Figure 2 shows sample output of the drainage and divide networks extracted from a DEM of mountainous terrain in California. Field checking with Ames personnel revealed the techniques to be particularly effective in rugged terrain, with few significant errors occuring. Future work to be pursued with colleagues at Ames include extension of the techniques to regions with less rugged topography, improvement of the relational/spatial data base management routines and application to specific current and proposed NASA programs.

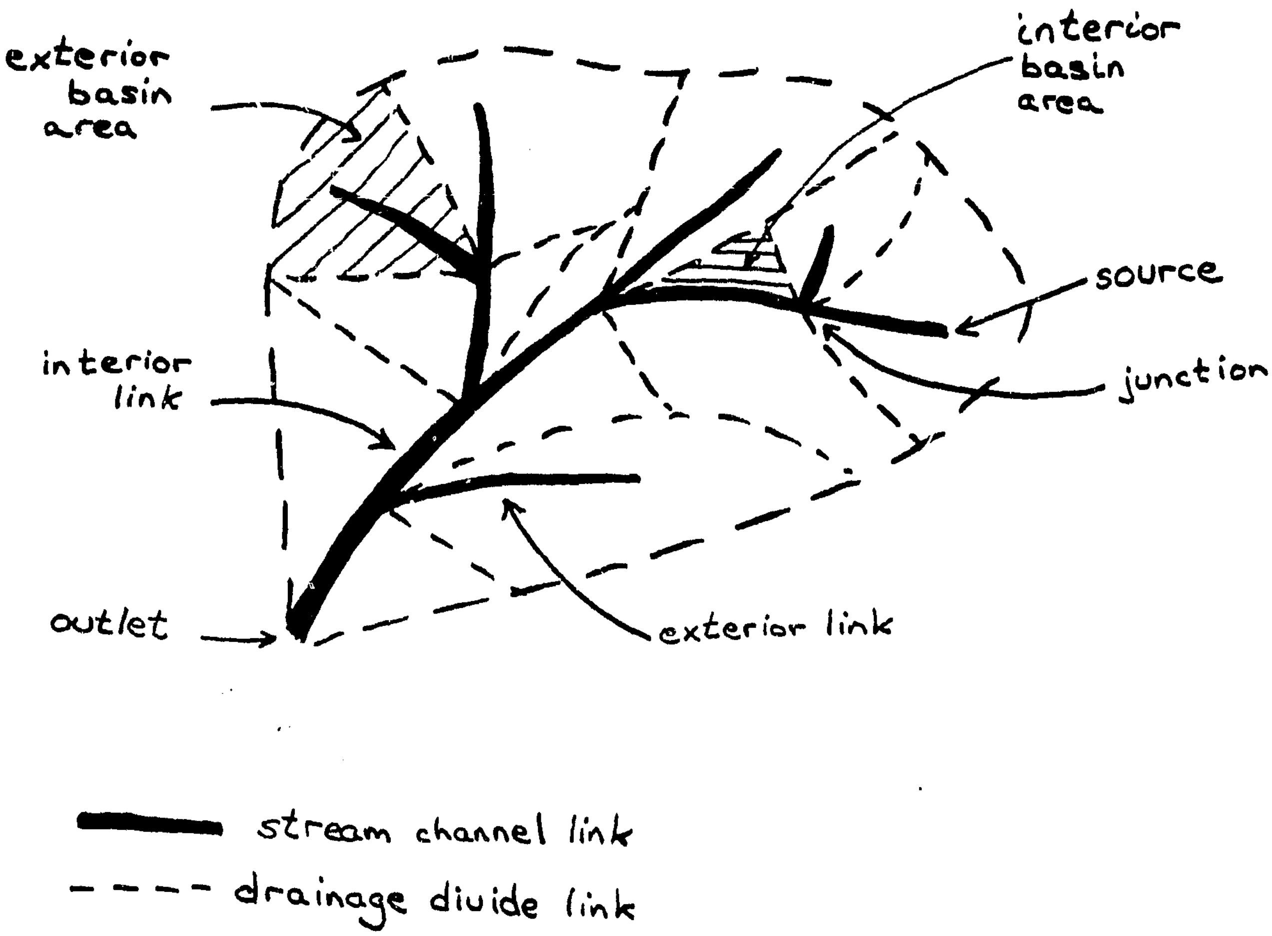

Figure 1: Complementary stream channel and drainage divide networks.

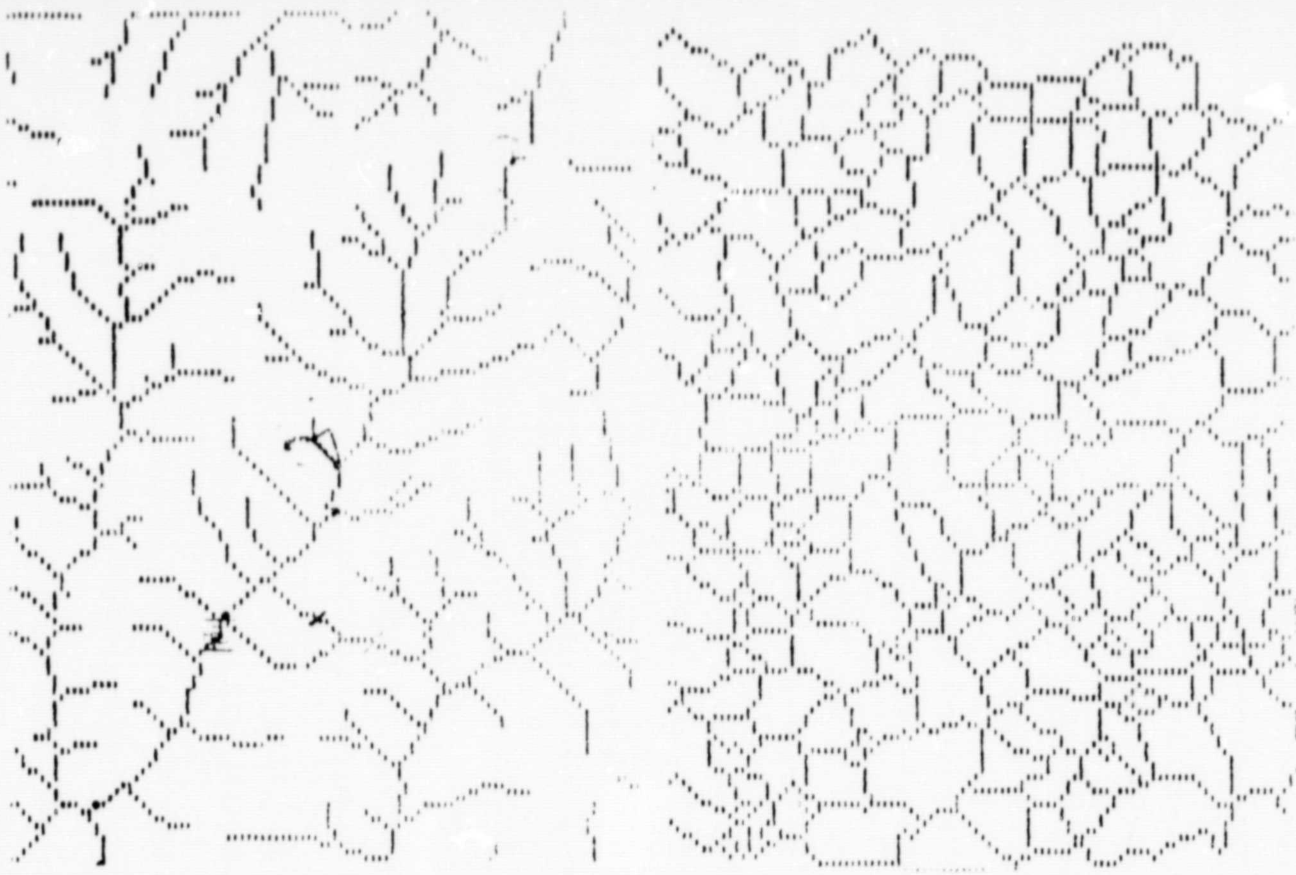

Figure 2: Examples of drainage channel and divide graphs for mountainous terrain in California.

ORIGINAL PAGE IS
OF POOR QUALITY

Plate I: Typical interior channel link in Mineral King channel network structure, Sierra Nevada.

Requirament for Torque Transducer
in Flight Simulators

Rose Marie Dishman
U.S. International University
Associate Professor of
Engineering/Science

Each NASA-ADFRF 3 axis flight simulator requires 3 DC torque motors. The motors provide force for the control stick (pitch axis and roll axis) and the rudder pedal (yaw axis).

New motors have been purchased which have many advantages over the original model, including higher torque, lower power requirements, and excellent resistance to demagnetization. However, the new motors exhibit higher cogging and magnetic friction. These effects are very noticeable to the pilot in the low force region.

My summer project was to find a suitable torque transducer to be permanently mounted on each motor to correct the problem. The torque transducer output will be used to electronically compensate for cogging/friction.

Physical configuration constraints were taken into account to minimize the redesign of the existing mechanical system. The position of the motor will remain fixed and the position of the pulley with respect to the motor will be the same. The pulley shaft will very likely be redesigned. The small space limits the size of the torque transducer to 4.0" long and 3.0" in diameter.

Some of the torque transducer specifications which must be met are:

I. The Torque Range
   A. Maximum torque with correct output is 400 in.-lb.
   B. The minimum readable torque output is .5 in.-lb.
   C. A maximum overload torque exists of 1200 in.-lb.

II. Direction of Torque
   A. The torque is applied in both directions and reverses direction frequently.
   B. The maximum peak-to-peak rotational angle is 315 degrees.

III. Accuracy
   A. Linearity: 3% of reading.
   B. Repeatability: 1% of reading.
   C. Stability of the zero point is essential (.1% of full scale).
   D. Good accuracy is needed in the region near zero.

IV. Other Specifications

A. Recalibration should be infrequent.

B. The transducer response should remain essentially flat to at least 50 Hertz.

The torque transducer is expected to use the strain gage bridge technique with a gage factor of 2 to 4 mV/V. The input voltage will be at least 10 volts.

After reseaching the problem, it has been determined that torque transducer technology does exist to meet the desired specifications. Several sources have been identified with existing commercial products that need minimal redesign. The estimated cost for 20 transducers including one time engineering development and production is $45,000.

The next step is to get two prototypes and then to develop the electronics necessary for the transducer output to compensate for the cogging/friction. By the end of summer 1985, torque transducers should be successfully electronically compensating for the cogging/friction in at least 6 DC torque motors.

Frequent discussions with Charles A. Wagner, my NASA-ADFRF colleague, provided excellent guidance and technical assistance.

REFERENCES

1. Musick, R.O. and Wagner, C.A., "A Flight Simulator Control System Using Electric Torque Motors", Presented at AIAA 13th Aerospace Sciences Meeting January 1975.

2. Norton H.N., Handbook of Transducers for Electronic Measuring Systems, Prentice-Hall, Inc. 1969.

3. ISA Transducer Compendium, 2nd Ed.-Part 2, Instrument Society of America 1970.

4. Discussions with and/or catalogue research of the following companies: AKO Inc., Ametek Instrument & Control Div., AMTI, Brewer Engineering, D.J. Instruments Inc., Eaton Corp.(Lebow Products), Engineering Specifics Assc., GSE Inc., Hottinger Baldwin Measurements, Inland Motors, Interlaken Tech. Corp., Kaman Instruments, McFadden Systems, S. Himmelstein, TEDEA, Torque & Tension Equipment Inc., Vibrac Corp., West Coast Research.

CONTROL ENHANCEMENT USING JET VANES

Donald W. Kelton, Highline College

Purpose:

This study examines the effectiveness of utilizing a vane, deflected into the exhaust stream of a jet engine, in inducing forces and generating moments which can move or control the movement of aircraft.

Areas of, and Reasons for Interest

1. Spin recovery - There have been instances where operational aircraft (fighters) have gone into flat spins and have been unable to recover using their existing control modes. A jet vane would be completely functional as long as the engine were not stalled out.

2. Supermaneuverability - Operations analyses of fighter combat using short-range all-aspect air-to-air missiles now in development suggest need to quickly point and shoot, and have defined unusual maneuvers which will consistently defeat the currently favored tactic of pulling the tightest possible turn. These tactics involve pitching up to extreme angles of attack, well beyond the stall boundary, then yawing severely to dive down on the adversary. (Ref. 6,7,8)

Navy studies (Ref. 2) indicate that the maneuvering enhancement from utilizing jet vanes can provide a 4 to 1 margin in "time-on" (i.e., in position to sucessfully fire upon adversary) in representative fighter encounters.

3. Tailless aircraft - Future conceptual aircraft configured without conventional aerodynamic tail surfaces for stability and control have been proposed. Possible advantages offered are reduced drag and control simplification. A large scale test has been conducted in the Langley 30' x 60' tunnel with a tailless aircraft and both stability and control were demonstrated up to angles of attack of 90°.

Scope of Study:

The effort this summer has been to investigate the feasibility of employing a jet vane for yaw control. The yaw axis was chosen for two reasons: (1) applicability to spin recovery and (2) relative ease of mounting on several types of current fighters.

The study involved the following main avenues:

1. Obtain tailpipe exit jet stream data from a representative jet engine (used G.E. F-404 turbofan, engine of the F-18) to determine unit forces which can be produced on the vane. Examine various Mach No./altitude flight conditions.

2. Examine thermal effects - Determine temperature of gas on hot side. Select materials capable of strength retention at elevated temperatures. Obtain computer analysis of time-temperature-thickness variation for various materials, various flight conditions.

3. Determine vane size through extracting data on airplane characteristics and derivatives and engine parameters from flight simulator runs, wherein a flat spin was established and recovery initiated.

4. Examine configuration parameters for design and installation of jet vane.

   a. Possible installations when jets are widely spaced or closely placed.

   b. Requirements for two axis (pitch as well as yaw) system.

   c. Possible actuation methods.

References

1. "Jet Engine Thrust Turning by the Use of Small Externally Mounted Vanes" David W. Lacey and Richard D. Murphy, Jan 83, David W. Taylor Naval Ship Research and Development Center.

2. Thrust Vane Maneuvering Device for Tactical Aircraft Presentation Charts D7NSRDC.

3. Computer Program 80031A Users Manual (U) F404 Engine SC Memo 80 SC 31A, 26 Aug 81. General Electric Aircraft Engine Group, Lynn MA.

4. Model Specification for F-404-GE-400 Turbofan Engine, General Electric Aircraft Engine Group, Lynn, MA.

5. Equations, Tables and Charts for Compressible Flow, NACA Report 1135.

6. Supermaneuverability, W.B. Herbst PUB/120, 7 OCT 83, Messerschmitt-Bolkow-Blohm.

7. Military Advantages of Supersonic Maneuver, W. B. Herbst, 10-13 Oct 83, paper: Symposium on Technology for Sustained Supersonic Cruise and Maneuverability.

8. Future Fighter Maneuverability for Air Combat, W. B. Herbst, AIAA paper, Ft. Worth, Texas 17-19 Oct 83.

Yaw Control Vanes

NASA
AD84-1003

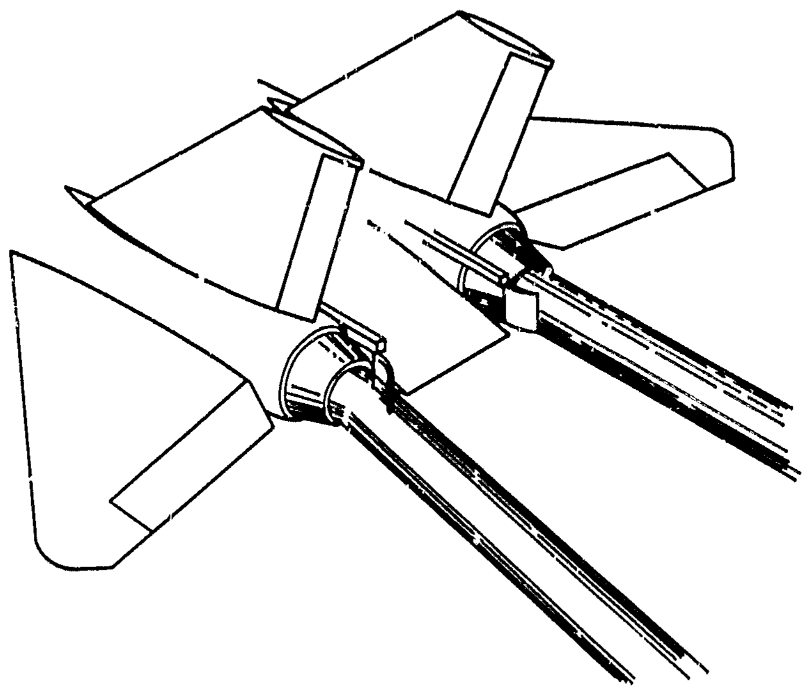

Vane Force Versus Deflection Angle

NASA
AD84-988

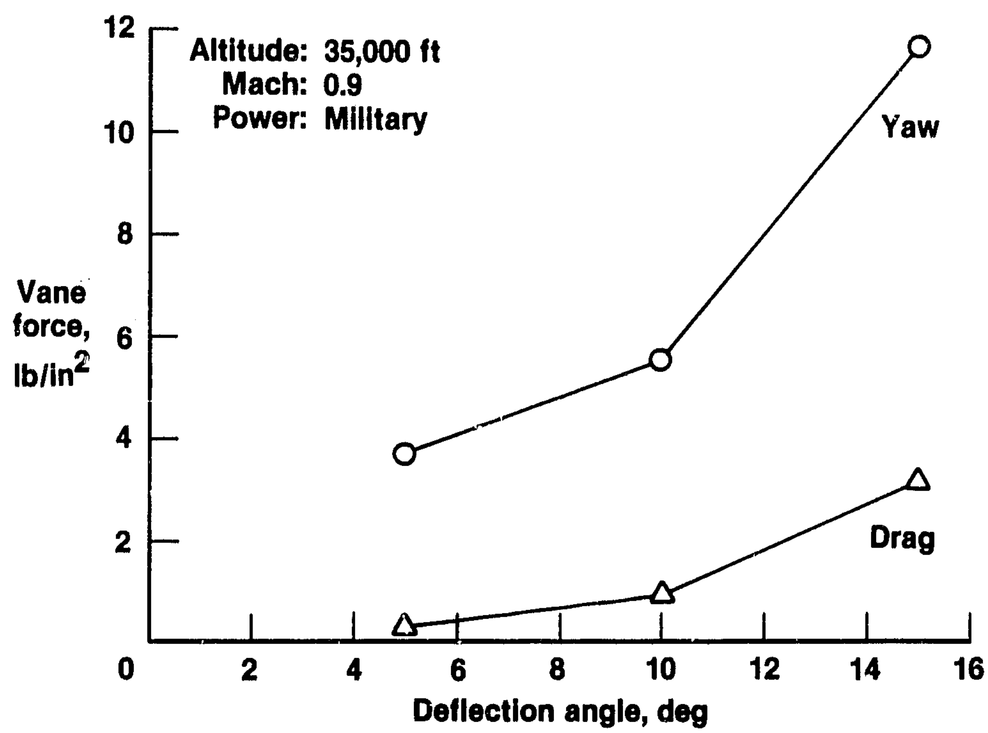

Efficient Analytic Computation of Derivatives of the Potential Energy Surface for Small Molecules or Molecular Clusters

Harry King

State University of New York at Buffalo

Professor of Chemistry

The energy of a molecule or of a molecular cluster is described by its potential energy surface (PES), a quantity which is of fundamental importance for a wide variety of chemical problems such as for the prediction of chemical reactions and optical properties of molecules in shock fronts created by a reentry vehicle. Typical molecular vibrations correspond to small amplitude vibrations in the vicinity of a minimum on the PES, and infrared spectra correspond to transitions between quantized states of such motion. For this application one is particularly interested in the curvature of the surface at the bottom of a potential well, i.e. second derivatives of the energy with respect to displacements of nuclei from their equilibrium positions. A chemical reaction corresponds to motion from one local minimum on a PES to another. The rate of the chemical reaction is profoundly affected by the location and height of the transition state, i.e. the saddle point connecting these two local minima. The computational problem of finding such transition states is significantly reduced if one can compute not only the energy for a given geometrical arrangement of nuclei but also derivatives of that energy.

For a molecule with N nuclei the PES is a function of 3N independent variables,

$$E = E(x1,y1,z1,x2,y2,\ldots,yN,zN)$$

where (xK,yK,zK) are the three cartesian coordinates of the Kth nucleus. At any point on the surface, i.e. for a specified set of 3N coordinates, the value of the energy ,E, is given by solving the electronic Schroedinger equation. This itself is a formidable computational problem that has been addressed in thousands of articles in the scientific literature. The equations are never solved exactly, but from theory and experience one knows pretty well

ORIGINAL PAGE IS
OF POOR QUALITY

how much accuracy to expect from various approximate solutions. The computational chemistry group at Ames is one of the world's leading centers for this work, and they have developed state-of-the-art computer codes on the Cray and Cyber supercomputers for molecular electronic structure calculations. With the exception of one such code called GRADSCF these programs all compute the PES point by point. At the beginning of my project the GRADSCF codes were capable of computing first derivatives of the energy within the self-consistent-field approximation to the Schroedinger equation, i.e.

$$G = dE/dx$$

My project is to extend this to second derivatives. The technology for this has, in fact, already been developed at other institutions. My own research group at Buffalo has devoted several man years of effort to the development of closely related codes, but for various reasons we undertook the task of writing an entirely new computer program. It is structured to be more compatible with existing codes at Ames, better suited to the vector processing capabilities of the Cray computer, and organized with a view toward use with other more accurate approximations to the true solution of the Schroedinger equation such as the MCSCF and CI formalisms.

The quantum mechanical expression for the electronic energy has been differentiated analytically and cast in a convenient mathematical form for computation. This reduces to an arduous exercise in calculus. A few thousand lines of new code were written during the summer for evaluating the resulting formulas. Just as this first summer draws to a close the computer program has been completed and tested and found to give results in agreement with previous results obtained at Ames from a series of point-by-point computations. Thus we are confident that our mathematics is correct. Much remains to be done to improve computational efficiency and to enable the program to handle larger molecules. The program will then be linked up with other programs to compute infrared spectral properties and to search for transition states.

Although I have devoted much of my professional lifetime to computational problems in chemistry, I had no previous experience the Cray or with vector machines in general. So this has been an entirely new aspect for me. I have worked closely with Dr Andrew Komornicki throughout the summer and he has accepted the greatest part of the burden of educating me in all this, but Drs. David Cooper, Charles Bauschlicker, Richard Jaffe, and others have also been very helpfull not only with computational matters but also in giving me some insight into the general methods and applications being pursued within the computational chemistry group at Ames.

I hope to continue this work next year. Just working out the calculus and producing a working computer program has required an intensive effort which left little time for thinking about chemistry. Like a boy with a new knife looking about for a good piece of carving wood, I look forward to seeing the program applied to the solution of an actual chemical problem.

Fault Tolerant Features of RAMPS (Redundant Asynchronous Microprocessor System)

Stella Lawrence
Professor

Bronx Community College of the City University of New York

RAMPS is the architectural structure of the hardware for UFTCS (Ultrareliable Fault Tolerant Control System). In fault tolerant systems, decisions depend upon a redundant logic majority vote. The basic criteria are that the redundant system elements must be independent and the redundantly generated outputs must be unambiguous.

RAMPS consists of n, autonomous, asynchronous computers in parallel. The asynchronous system elements have a knowledge of real time and therefore generate outputs that can be correlated on the basis of amplitude and time.

Systems with free integrators have control algorithms that are not asymptotically stable. The independent, parallel computers are subject to digitizing delays, and for a unit step input the two computers showed a constant discrepancy in value. Simulation demonstrated that if a lag element (filter) were substituted for the integrator the two outputs converged in time. Furthermore, since the Laplace transform for the lag is $1/(s+w)$, and the Laplace tranform for the integrator is $1/s$, the lag circuit approaches the integrator as w approaches zero.

My project was to solve the problem analytically. I had to determine the correct representation of the control loop, which involved an analog input, A/D conversion, sampling, sample and hold circuits, and D/A conversion, obtain the system outputs $y(t)$ and the computer outputs $f(k)$, determine whether they converged and if so, how rapidly.

RAMPS essentially involves a hybrid, sampled-data negative feedback system. The system is a hybrid system because the analog input is sampled and undergoes A/D conversion. The computer represents a discrete system and the plant (the helicopter) a continuous system. The system was modelled mathematically via the z-transform. (The z-transform converts difference equations to algebraic equations). With the z-transform the response values for the continuous system are given only at the sampling instants, 0,T,2T, etc. the second computer may be considered to be delayed in time: ΔT, $T+\Delta T$, $2T+\Delta T$, etc. To obtain the response within the sampling interval $t=\Delta T$, (between 0 and T), for the second computer, the advanced z-transform was used.

For the first computer:

$$Y(z)/R(Z) = G_c(z)G(z)/\left[1 + G_c(z)G(z)\right], \text{ and}$$

$$E(z) = Y(z)/G(z).$$

ORIGINAL PAGE IS
OF POOR QUALITY

For the delayed computer:

$$Y(z)/R(z) = G_c(z)G^*(z)/\left[1+G_c(z)G(z)\right]$$, where $G^*(z)$ represents the advanced z-transform.

The response to a unit step was found to be:

$$y(t) = 1 - ae^{-bt}\sin(ct + \phi),$$

where $G_c(s) = 1/s$, (integrator).

The response for the second computer (advanced z-transform) was found to be:

$$y(t) = e^{-\Delta T} - ae^{-bt}e^{-\Delta T}\sin(ct + \phi),$$ as

$T \rightarrow 0$, $e^{-\Delta T} \rightarrow 1$, and the two responses coincide.

The computer output was found to be $1 + me^{-bt}\sin(ct + \phi)$.

Further work is required:

1) to determine the response of the system to a unit step, (and to other inputs), for a filter (or lag function):

$$G_c(s) = 1/(s+w),$$

2) for further theoretical control loop analysis of the system.

In addition, the inverse z-transform is usually obtained from the table of inverse z-transforms via partial fraction expansion. Computer programs should be developed to calculate the value of the resulting infinite series when the inverse z-transform is obtained by means of the long division of two polynomials. The LCAP program (Linear Control Analysis Program) should also be applied to help with the polynomial subroutines involved in determining the inverse z-transform.

I found the work on the project stimulating and rewarding. I greatly enjoyed working with Dr. Larry Webster under the direction of Branch Chief Dr. John Bull. Dr. Jim Howard was also very helpful. Everyone was very kind and cooperative including Peggy Brown, Elaine Larsen, and the Library Staff.

References

1. Jury, E. I., Sampled Data Control Systems, John Wiley and Sons, New York City, 1958.
2. Jury, E. I., Theory and Application of the Z-Transform Method, John Wiley and Sons, New York City, 1964.
3. Sklansky, J., Network Compensation of Error Sampled Feedback Systems, Technical Report No. T-1!B, Columbia University, New York, April 1955.
4. Baker, R. H., The Pulse Transfer Function and Its Application to Sampling, Proceedings IEE, Vol. 99, Part IV, Dec. 1952.
5. Lathi, B. P., Signal, Systems and Control, Intext Educational Publishers, New York 1974.
6. Eveleigh, Virgil W., Introduction to Control Systems Design, McGraw Hill Book Company, New York 1972.
7. Heffley, R. K., Jewell, W. F., Whitbeck, R. F., Schulman, T. M., Analysis of Delays in Simulator Digital Computing Systems SRI Technical Report, No. 1140-L-1m, Systems Technology, Inc., Bayshore Frontage Road, Mountain View, CA 94943, Contract NAS2-10106 NASA Ames.
8. Saucedo, R. and Schiring, E. A., Introduction to Continuous and Digital Control Systems, Macmillan, New York 1968.
9. Saltzer, J. M., Sampled Data Theory, Intellectronics Laboratories, Ramo Wooldridge Div., Thompson., Thompson Ramo Wooldridge, Canoga Park, CA in the book by Leonides, C. T., Computer Control Systems Technology, McGraw Hill Book Co., New York, 1961.

Fig. 1

Hybrid, Negative Feedback Sampled Data System

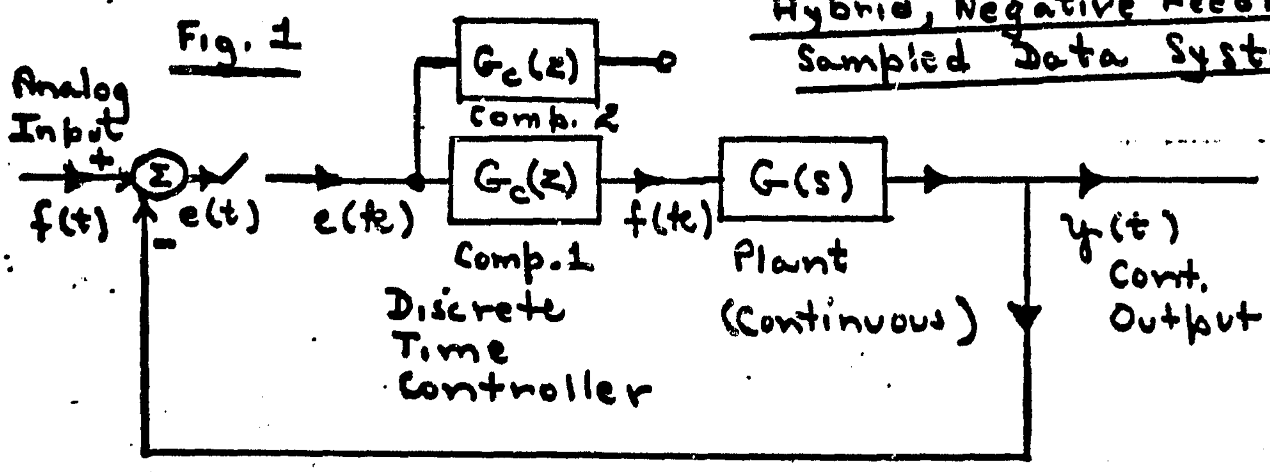

Fig. 2

Computer Outputs (Simulation)

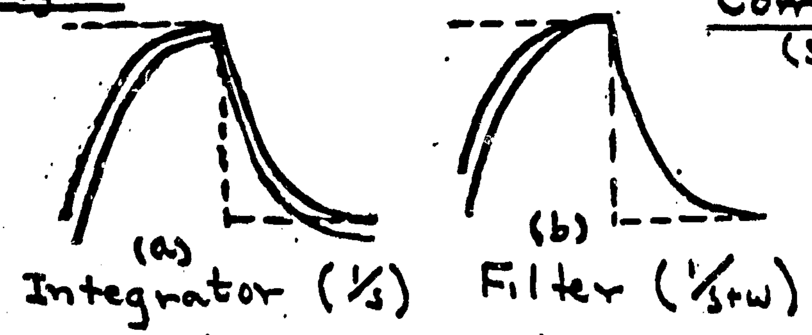

Fig. 1

Hybrid, Negative Feedback Sampled Data System

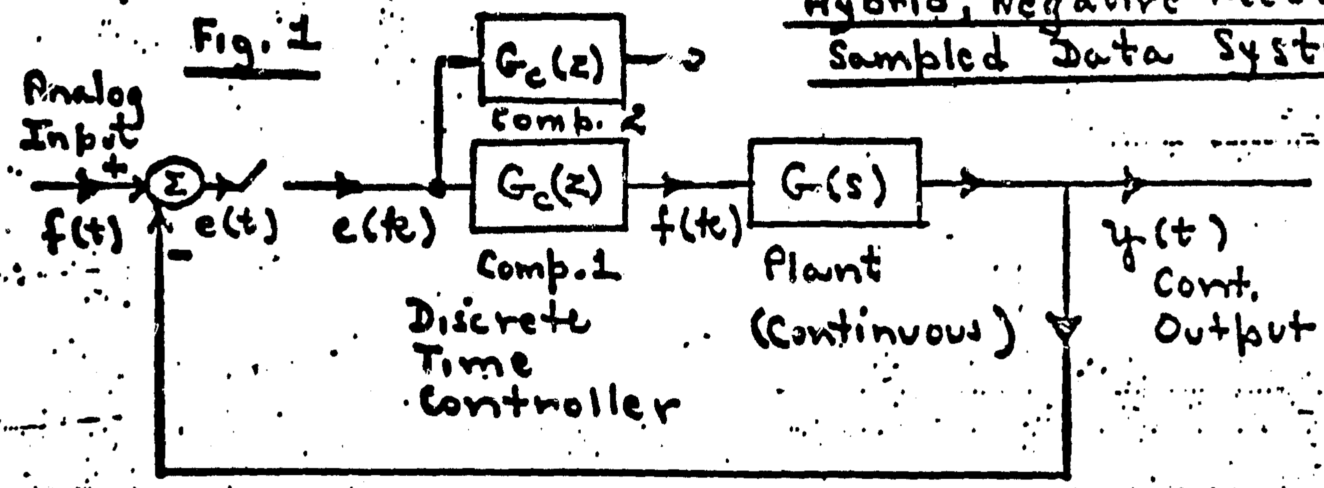

Fig. 2

Computer Outputs (simulator)

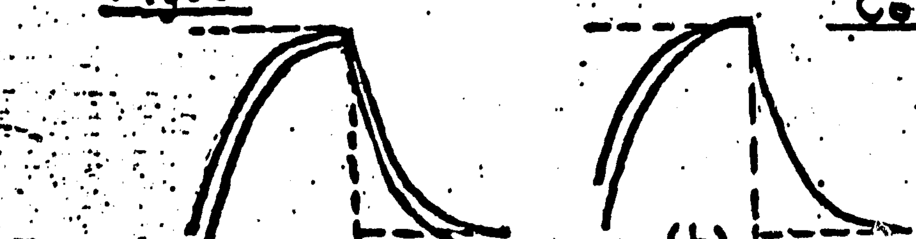

(a) Integrator (1/s)

(b) Filter (1/(s+w))

References

1. Jury, E. I., Sampled Data Control Systems, John Wiley and Sons, New York City, 1958.
2. Jury, E. I., Theory and Application of the Z-Transform Method, John Wiley and Sons, New York City, 1964.
3. Sklansky, J., Network Compensation of Error Sampled Feedback Systems, Technical Report No. T-11B, Columbia University, New York, April 1955.
4. Baker, R. H., The Pulse Transfer Function and Its Application to Sampling, Proceedings IEE, Vol. 99, Part IV, Dec. 1952.
5. Lathi, B. P., Signal, Systems and Control, Intext Educational Publishers, New York 1974.
6. Eveleigh, Virgil W., Introduction to Control Systems Design, McGraw Hill Book Company, New York 1972.
7. Heffley, R. K., Jewell, W. F., Whitbeck, R. F., Schulman, T. M., Analysis of Delays in Simulator Digital Computing Systems SRI Technical Report, No. 1140-L-1m, Systems Technology, Inc., Bayshore Frontage Road, Mountain View, CA 94943, Contract NAS2-10106 NASA Ames.
8. Saucedo, R. and Schiring, E. A., Introduction to Continuous and Digital Control Systems, Macmillan, New York 1968.
9. Saltzer, J. M., Sampled Data Theory, Intellectronics Laboratories, Ramo Wooldridge Div., Thompson., Thompson Ramo Wooldridge, Canoga Park, CA in the book by Leonides, C. T., Computer Control Systems Technology, McGraw Hill Book Co., New York, 1961.

Development of Finite Element
Numerical Methods and Its Applications
to the X-29A Aircraft

By John B. Mckinney, P.E.

Cal Poly Pomona
Associate Professor of Engineering Technology

An Aerospace Structural Engineer is faced with the difficult task of designing a lightweight structure that can withstand the severe static and dynamic loading conditions imposed on such structures. In particular the X-29A is an advanced concept prototype fighter of the 1990's, which utilizes forward swept wings and composite construction.

The Aerostructures group of the Ames Dryden Flight Research Facility to which I am assigned is responsible for the structural analysis of the X-29A, specifically, I worked on the structural dynamics of the forward swept wing.

In general, because aircraft structures are so complex and the accuracy of any analysis is paramount, the Finite Element Method is used to do the structural analysis. In the static case, we are concerned with internal forces, stresses, and deflections. In the dynamic case we look at the natural frequency and mode shapes of the structure which become an essential part of the flutter analysis.

In order to obtain such results for the forward swept wing of the X-29A, we modeled the composite upper and lower wing surfaces and internal structure as being structurally equivalent to a plate element incorporating beam elements around its edges. In all, it took 981 elements to model the semi-span of the X-29A wing.

In order to solve for the free vibration analysis of the wing, the STARS program was utilized. In this program the well known differential equation of motion for a damped structure, $KU + C\dot{U} + M\ddot{U} = 0$, is reduced in matrix form to the solution of the eigenproblem, $(K - \lambda^{2}M)y = 0$, in which M and K are the mass and stiffness matrices, λ is the eigenvalue which is related to the natural frequency by $\omega = \sqrt{\lambda}$ and y being the eigenvector which gives us the mode shapes.

Because the wing and for that matter, most all aerospace structures have rather large associated mass and stiffness matrices, the solution of the eigenproblem can be rather time consuming in terms of computer time.

In order to reduce the solution time, we have come up with an improved numerical technique for finding eigenvalues and associated eigenvectors. In the old method the roots (eigenvalues) were first isolated by a repeated bisection procedure and Sturm sequence count after which the roots and vectors are determined by an inverse iteration method. In the new method the roots are isolated as before and at the same time the roots and vectors are determined simultaneously. As a result, the solution times have been reduced by 30% to 50%.

The attached figure shows both the undeformed structure (solid lines) and the shape of the first mode (dotted lines) for the x-29a. Also included therein are the natural frequencies of the first six modes, up to 15 modes have been successfully found using this new method with a substantial savings in time.

References

Gupta, K.K., 1983, STARS, A General Purpose Finite Element Computer Program for Analysis of Engineering Structures.

IODE NO. 1 f = 10.31 Hz.

TABLE 1. Free Vibration Analysis Results of the X-29A Wing Model

Mode No.	Natural Frequency (Hz)
1	10.3099
2	23.5088
3	41.4439
4	43.7517
5	69.2642
6	77.8427

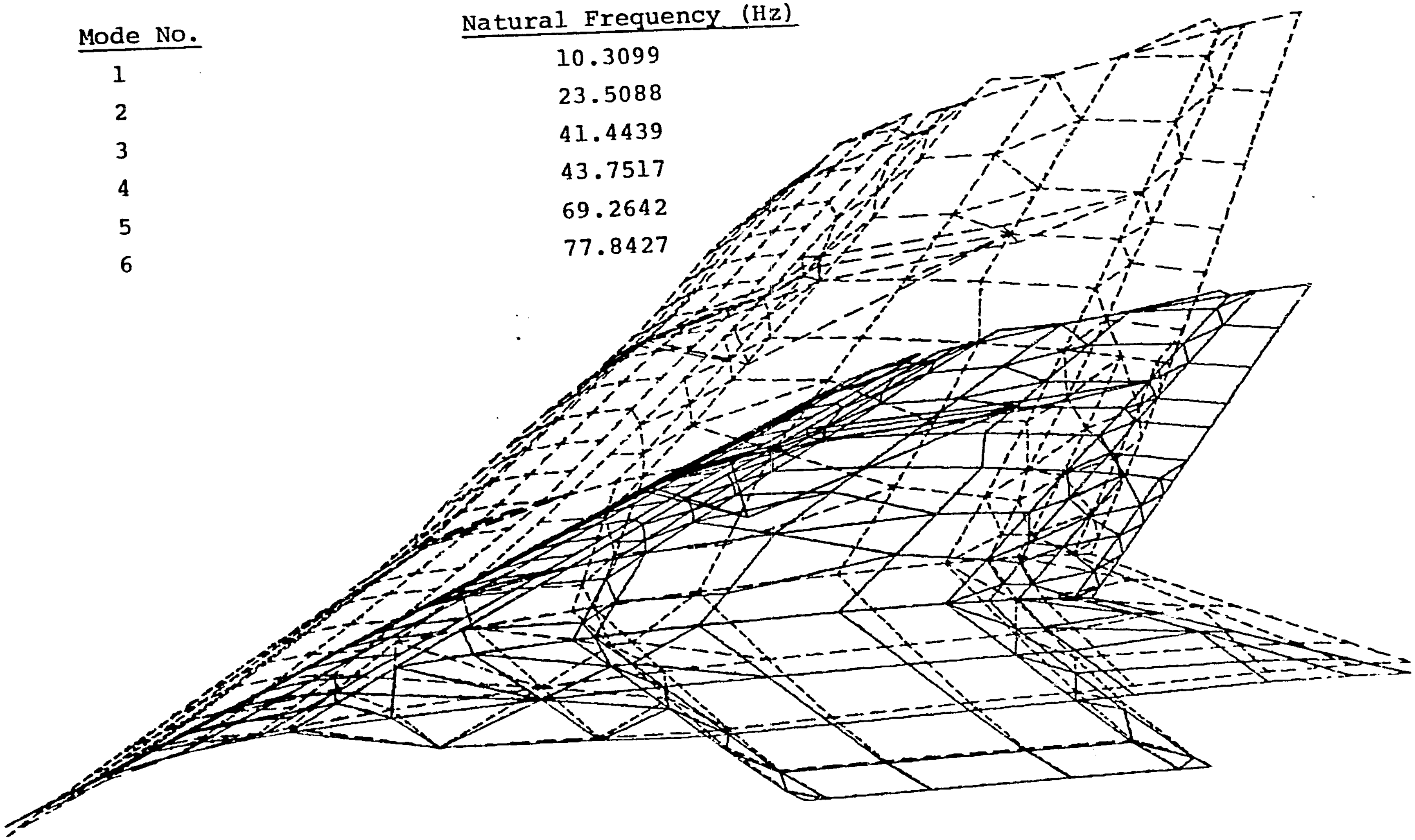

Figure 1 - FSW Aircraft Wing Mode Shape

Characterization of the DNA from the Cyanelles of Glaucocystis nostochinearum

O. Tacheeni Scott
Northern Arizona University
Assistant Professor of Biology

My proposed project for the summer entailed the determination of the genomic size of the cyanelles of the enigmatic "algae" Glaucocystis. For a century, Glaucocystis successfully defied a taxonomic assignment within established algal systematics. It has been assigned at various times to the Schizophyceae ("blue-green algae"), red algae, dinoflagellates, green algae, and Glaucocystideae, a sub-class created for the taxonomic recognition of algae similar to Glaucocystis. A German researcher proposed in 1923 that Glaucocystis represented an endosymbiotic association involving intracellular cyanobacteria and a colorless green algal host. Few accepted Geitler's idea and the taxonomic position of Glaucocystis remained unsettled until the present year. I and my former Ph.D. advisors published the first unequivocal argument that Glaucocystis is indeed a unique association of cyanobacteria (= cyanelles) and a colorless plant cell, probably of the green algal group (eukaryotic).

If the endosymbiotic argument is to be substantiated beyond the remnant bacterial cell wall argument that I presented (Arch. Microbiol., late summer, 1984), I must be able to demonstrate additional arguments that the endosymbiont is truly a former cyanobacterium which is still identifiable as a prokaryote. Therefore, I came to NASA-Ames with the idea that I wanted to isolate the DNA from the cyanelle and to attempt to determine its molecular weight. My reason for wanting to do this was simple: Is the genome 10^8 or 10^9 daltons? If the molecular weight is closer to the lower value, then the endosymbiont could be argued to have lost some of its DNA since assuming the intracellular position. If the the value is closer to the higher number, then my argument that the cyanelles is STILL identifiable, based on DNA content, as a bonafide photosynthetic prokaryote.

The project was slow in getting off the ground because my cultures were not in the best physiological condition in late June. I had not worked with Glaucocystis in over 4 years and I had decided to get around its slow growth by attempting to grow it in several novel fashions including bubbler cultures, shaker culture, agar cultures, and "spinner-bottle" cultures. The association is slow-growing and the summer simply slipped by before I had enough healthy cells to work with. The host cell must be fractioned with a glass tissue homogenizer in order to free the cyanelles for isolation work.

I used standard molecular biology methods to isolate the cyanelle DNA. I was not however able to perform agarose gel eletrophoresis for the purpose of getting a rough first order idea of the molecular weight. I also attempted to isolate a plasmid fraction. The fractions are in buffer at this time and will have to be determined when I return to my institution.

The summer was not lost however as I gained insight in many valuable discussion with NASA personnel and researchers at other universities who presented seminars at both Ames and San José State University where the NASA-sponsored Planetary Biology course was taught this summer. I was able to present a formal seminar at NASA in July. I received a good response and was encouraged by NASA's interest in Glaucocystis.

Vorticity Interaction
The Measurement of Vortex Strength

H. Jerome Shafer
Technion-Israel Institute of Techlology

The blade-vortex interaction problem, being of a most complex nature, can probably be best understood by gaining an insight into the basic phenomena of which the problem is composed. The Stanford Aero/Astro Dept. study of vorticity interaction* proposes to study single vortices produced by a shock tube in an effort to gain a fundamental understanding of vortices per se, especially in the compressible flow regime and then to study how these vortices interact with solid boundaries.

The shock wave leaving an open ended shock tube is followed by a flow of the gas traversed by the shock wave in traveling down the tube. In the current investigation both the shock and the flow are confined in one direction normal to the flow direction by transparent plastic walls which as act as extensions of one set of walls of the shock tube. The shock and the gas are free to expand and flow in the other direction normal to the axis of the shock tube. A pair of symmetrical vortices are generated at the abrupt opening of the shock tube by the outflowing gas. A picture of the density at each point in the field is obtained by holographic interferometry. In this technique a double exposure hologram is made, first a tare exposure and then an exposure of the phenomenon. A photograph of the reconstructed hologram gives a picture of constant density contours over the whole field, identical with the isopycnal technique of conventional interferometry.

One of the basic quantities needed to be determined in this study is the strength of the generated vortex. This can be accomplished by measuring the tangential velocity of the fluid in the vortex and its radial distribution. Because of the transient nature of the phenomena in the current investigation only velocity measuring methods of high frequency response can be used.

Two possible methods of measuring the transential velocity are the Laser Doppler Anemometer (LDA) and the Hot Wire Anemometer (HWA). Both of these methods which measure at a "point" will require a previous knowledge of the vortex trajectory so that the HWA probe or the LDA measuring volume can be placed prior to shock tube firing. There is no possibility of optimizing adjustment during the actual experiment. The times involved in individual experiments are of the order of tenths of a millisecond.

The LDA has certain inherent advantages: it is nonintrusive and as such does not interfere with phenomena under study; it has no elements that can be damaged by the flow; it measures velocity directly. Seeding seems to present no problems. It has been shown* that dust particles of 0.1μm to 0.1μm require a time of about 4 μsec to be accelerated to full flow velocity after the passage of a shock wave of $M_s = 1.4$ ($V_2 \approx 200$ m/sec). However, two problems tend to mitigate against the use of LDA: 1) its use simultaneously with the holographic interferometry would be complicated, (2) it would require equipment not readily available in the shock tube laboratory.

H.W.A., while being readily available in the shock tube laboratory has certain inherent disadvantages: 1) it requires an intruding sensor which may interfere

---

*Bershader, D., Progress Report & Proposal for Continuation of a Vorticity Interaction Study; Dept. of Aero/Astro, Stanford University, July 1984.

**von Stein, H.O. and Pfiefer, H.J., "Investigation of the Velocity Relaxation of Micro-Sized Particles in Shock Waves Using Laser Radiation"; Applied Optics, Vol. 11 #2, Feb. 1972, pp. 305-307.

with the flow, 2) the delicate wire on the probe can be easily damaged, 3) it measures mass flow rather than velocity directly, 4) it may present problems in determining relative flow direction especially in the transonic regime. The overcoming of these diffidulties is a major part of the effort to measure the radial distribution of the tangential velocity of the fluid in the vortices.

In the shock tube experiments, as mentioned above, two symmetrical vortices are formed. One will be used as a reference and the other will be "experimented" with. A splitter plate placed mid-way between the vortices along the axis of the shock tube will prevent interaction between the vortices even when one is being "experimented" with. In a preliminary experiment a H.W. probe were placed at some predetermined position relative to the trajectory at one of the vortices and an interferogram of the complete flow field was made at such a time that interaction between probe and vortex has taken place. The two portions of the interferogram – the undisturbed vortex and "experimented" vortex would be compared to determine the extent of the interaction. The H.W.A. probe has been examined to determine how well it holds up mechanically under the forces imposed by the shock wave and flow. There seems to be no problem in that respect.

It is anticipated that the main mechanical problem will be wire breakage. This can probably be overcome by the use of epoxy-backed sensors such as have been developed at Ames. Experience there has shown that the epoxy backing may not affect the operation or characteristics of the wire. *Robinson, et al reports "the epoxy-backed wire, which is useful in high speed flows because of its improved strength gave very similar results to the free "hot-wire". The added rigidity also enables a more precise determination of relative angle between flow and wire. Arrangements have been made to have such epoxy-backed hot-wires made at Ames.

One of the main problems in using HWA to measure velocity in compressible flow is the fact that the HWA responds to mass flow and temperature. In the incompressible flow regime changes in flow velocity are not accompanied by changes in density or temperature and hence the constant value of these quantities can be combined into a calibration constant. The determination of velocity then follows simply from a direct calibration of bridge current or voltage at a function of velocity. In the compressible flow regime changes in velocity are accompanied by changes in both density and temperature. Special calibration and operating procedures such as repeated measurements at several overheated ratios must be followed to allow the separation of the several variables.

Horstman and Rose** have shown that sensitivity of the hot-wire to ambient temperature variations is reduced by operating the wires at as high an over-heat ratio as possible. An additional advantage to operating at high over-heat ratios is that the density sensitivity and velocity sensitivity ratio is constant. In the proposed study this is an advantage since density can be determined

---

*Robinson, S.K., Seegmiller, H.L. & Kussog, M.E.; Hot-Wire & Laser Doppler Anemometer Measurements in a Supersonic Boundary Layer, AIAA Paper AIAA 83-1723; Danvers, Massachusetts, July 1983.

** Horstman, C.C. & Rose, W.D., Hot-Wire Anemometry in Transonic Flow, NASA TM.X-62495, December 1975.

independently from the interferograms which allow a direct determination of the density at every point in the field at the instant at which the second exposure of the hologram is made. A series of independent interferograms made at time lags of several tens of microseconds apart will enable a time history of the complete density field to be made. Densities so determined can be used to obtain velocity from the HWA mass flow measurements.

The technique proposed to measure the tangential velocities is that of the X probe. The probe is set parallel to the shock tube so that the X is symmetrically oriented with reference to the horizontal velocity vector. By subtracting the signal of one wire from the other the normal velocity component of the complete flow will be determined, i.e., tangential velocity of the vortex plus or minus the normal component of the mean flow velocity. The tangential vortex velocity in the direction normal to the shock tube will change direction after transversing the vortex core while the normal velocity of the general flow will continue in the same direction. Assuming a symmetrical vortex the vortex tangential velocity can then be determined by subtracting measured combined velocity symmetrically oriented with respect to the vortex core.

The effect of the angle ϕ between the flow velocity vector and the normal to a hot wire is given by $\cos^m\phi$, where m is a function of Mach number M, Smits to Muck* show that $m = 0.5$ for $M < 0.5$; $m = 1.2$ for $M > 2$. In the range $0.8 < M < 1.5$ m is a rapidly varying function of M. Since the whole technique of decomposing velocity vectors with the HWA depends on $\cos^m\phi$, the Mach number dependence of m will have to be investigated further and appropriate calibration procedures developed.

Despite the many problems in using the HWA to and in determining vortex strength it is felt that measurements can be made so as to further evaluate the magnitude of the various parameters with at least some moderate precision.

---

*Smits, A.J. and Muck, K.L., Constant Temperature Hot Wire Practice in Supersonic Flows, Part 2: The Inclined Wire; Experiments in Fluids 2, 1984, pp. 1-9

A Quadratically Convergent Scheme with a Large Degree of Parallelism for The Solution of Linear Matrix Equations

Dan Tylavsky
Arizona State University
Assistant Professor of Engineering

Solution of linear matrix equations by parallel methods is necessary if large problems which are of interest to NASA are to be solved. Parallel algorithms to solve these problems are, therefore, necessary. Methods which show superior performance are those which minimize precedence relationships. A good example of such a method is the quadratically convergent algorithm originally proposed by Hotelling [1943]. This method is, however, limited by the restriction that the eigenvalues of the iteration matrix have moduli which are less than 1.0. A quadratically convergent algorithm which has been investigated this summer is known as the Approximate Multiple Factorization (AMF) method. This method is superior to Hotelling's method in three ways.

1. The method converges to the identity matrix rather than the dense inverse matrix and hence, preserves sparsity in the iteration procedure.

2. The region of convergence of the method is substantially larger than Hotelling's method.

3. The method requires one matrix multiplication per iteration rather than two.

The AMF method is competitive with Hotelling's method in two ways.

1. The method is quadratically convergent.

2. Few precedence relationships exists since the method represents the inverse as a product of sparse matrix factors.

The first step in the AMF method is to order the coefficient matrix so that the largest matrix elements are located on or near the diagonal. The next step is to approximate the coefficient matrix as a block diagonal matrix by ignoring the off-diagonal elements. The inverse of this approximate matrix is then used as a preconditioner and will generate the sparsity pattern shown in (1).

$$\begin{bmatrix} A(1,1)^{-1} & & \\ & A(2,2)^{-1} & \\ & & A(3,3)^{-1} \end{bmatrix} \begin{bmatrix} A(1,1) & A(1,2) & A(1,3) \\ A(2,1) & A(2,2) & A(2,3) \\ A(3,1) & A(3,2) & A(3,3) \end{bmatrix} = \begin{bmatrix} I & \hat{A}(1,2) & \hat{A}(1,3) \\ \hat{A}(2,1) & I & \hat{A}(2,3) \\ \hat{A}(3,1) & \hat{A}(3,2) & I \end{bmatrix} \quad (1)$$

Notice that some fill-in will occur at this point in the algorithm. If the system of equations is loosely coupled then an approximate factorization of this matrix is,

$$
\begin{bmatrix} I & & \\ \hat{A}(2,1) & I & \\ \hat{A}(3,1) & & I \end{bmatrix}
\begin{bmatrix} I & & \\ & I & \\ & \hat{A}(3,2) & I \end{bmatrix}
\begin{bmatrix} I & \hat{A}(1,2) & \hat{A}(1,3) \\ & I & \\ & & I \end{bmatrix}
$$

$$
\begin{bmatrix} I & & \\ & I & \hat{A}(2,3) \\ & & I \end{bmatrix}
\approx
\begin{bmatrix} I & \hat{A}(1,2) & \hat{A}(1,3) \\ \hat{A}(2,1) & I & \hat{A}(2,3) \\ \hat{A}(3,1) & \hat{A}(3,2) & I \end{bmatrix}
\qquad (2)
$$

where the order of factorization is chosen arbitrarily. The effect of choosing this order in various ways is a subject of further research. Taking inverse of both sides of the (2) while ignoring the order of the factorization gives

$$
\begin{bmatrix} I & & \\ -\hat{A}(2,1) & I & \\ -\hat{A}(3,1) & & I \end{bmatrix}
\begin{bmatrix} I & & \\ & I & \\ & -\hat{A}(3,2) & I \end{bmatrix}
\begin{bmatrix} I & -\hat{A}(1,2) & -\hat{A}(1,3) \\ & I & \\ & & I \end{bmatrix}
$$

$$
\begin{bmatrix} I & & \\ & I & -\hat{A}(2,3) \\ & & I \end{bmatrix}
\approx
\begin{bmatrix} I & \hat{A}(1,2) & \hat{A}(1,3) \\ \hat{A}(2,1) & I & \hat{A}(2,3) \\ \hat{A}(3,1) & \hat{A}(3,2) & I \end{bmatrix}^{-1}
\qquad (3)
$$

Premultiplying the preconditioned coefficient matrix by the approximate inverse results in the following matrix.

$$
\begin{bmatrix} \tilde{A}(1,1) & \tilde{A}(1,2) & \tilde{A}(1,3) \\ \tilde{A}(2,1) & \tilde{A}(2,2) & \tilde{A}(2,3) \\ \tilde{A}(3,1) & \tilde{A}(3,2) & \tilde{A}(3,3) \end{bmatrix}
$$

This matrix will, from past numerical experiments, be a closer approximation to the identity matrix. If the procedure is repeated then the results at the end of the second iteration will be even closer to the identity matrix. Many numerical examples have been examined during the summer. One example which gives results which are typical of the algorithms performance, uses the matrix shown in (4). The tridiagonal matrix shown in (4) was chosen for this example since this type of matrix topography is typical of the matrices encountered in CFD type problems. The numerical entries were chosen to represent a particularly difficult problem which, though more extreme, is indicative of the CFD tridiagonal matrices which are neither diagonally dominant nor positive definite.

$$A=\begin{vmatrix}
1 & 20 \\
20 & 1 & 20 \\
& 20 & 1 & 20 \\
&& 20 & 1 & 20 \\
&&& 20 & 1 & 20 \\
&&&& 20 & 1 & 20 \\
&&&&& 20 & 1 & 20 \\
&&&&&& 20 & 1 & 20 \\
&&&&&&& 20 & 1 & 20 \\
&&&&&&&& 20 & 1 & 20 \\
&&&&&&&&& 20 & 1 & 20 \\
&&&&&&&&&& 20 & 1 & 20 \\
&&&&&&&&&&& 20 & 1 & 20 \\
&&&&&&&&&&&& 20 & 1 & 20 \\
&&&&&&&&&&&&& 20 & 1 & 20 \\
&&&&&&&&&&&&&& 20 & 1
\end{vmatrix} \tag{4}$$

The AMF method as described above was applied to this matrix by using 2 by 2 and 4 by 4 diagonal block preconditioners as shown in (1) and using approximate factors as shown in (2). The solution vector, x, was assumed to have all elements values equal to 1.0. This was then used to derive the b vector. A graph of the Euclidean error norm of the solution estimate versus iteration number is shown in Figure 1. This figure shows results for both the use of 2 by 2 and 4 by 4 diagonal block preconditioners. The important results to be taken from this figure are 1) the algorithm shows quadratic convergence characteristics and 2) the use of 2 by 2 diagonal block preconditioners has a slower initial convergence rate, but produces the converged solution in the same number of iterations. The second observation is important because when 2 by 2 preconditioners are used, the number of calculations which need to be performed are significantly less than when 4 by 4 preconditioners are used.

During this summer I have had many useful discussions with Ken Stevens about the role of parallel processing in the problems of interest to NASA. Based on these discussions I have plans to continue research on this method when I return to ASU, and to use the method presented as a preconditioning technique for use with conjugate gradient methods.

The second project in which I have participated, is the creation and submission of a research proposal to AFOSR for support of parallel

processing research on problems of interest to NASA. Cliff Rhoades and Ken Stevens have been particularly helpful by introducing me to potential sponsores at AFOSR and by aiding me in constructing a proposal which is not only of interest to AFOSR and me, but also of interest to NASA.

References

H. Hotelling, "Some New Methods in Matrix Calculation," Ann. Math. Stat., 14, (1943), pp. 1-34.

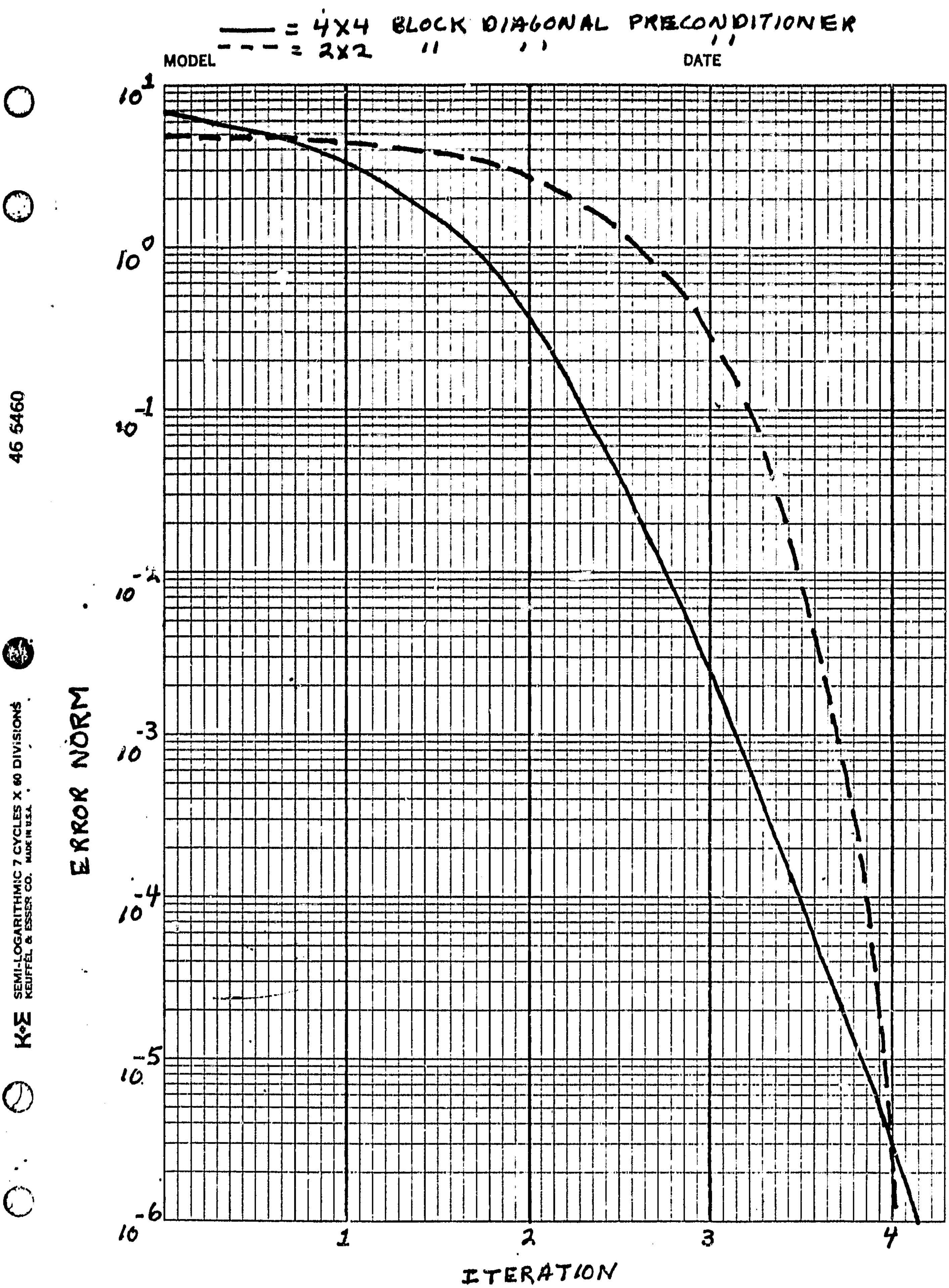

FIGURE 1: EUCLIDEA NORM OF SOLUTION VECTOR ERROR VERSUS IT[illegible]ATION NUMBER

WING/VORTEX INTERACTION

Sam Ventres
Associate Professor
Boston University

Unlike most NASA-ASEE Summer Faculty Fellows, I had not selected or been assigned a project when I arrived at Ames in June. My NASA colleague, Dr. Charles A. Smith of the Low Speed Aircraft Research Branch, had given me a list of topic areas of interest to his Branch, and I spent most of the summer selecting from these a subject of interest to me, and designing a project appropriate to my background and to the time and resources available for the job. This required a considerable amount of reading, and numerous conversations with NASA personnel, most of whom where in the Low Speed Aircraft Research Branch or in the Army Aeromechanics Laboratory.

It was established at the outset that, should a suitable project be agreed upon, funds would be provided by NASA for continuing the work at Boston University during the forthcoming academic year.

The project agreed upon is a computational investigation of the interaction of a convected line vortex with a wing of finite span. The line vortex is initially straight and is aligned with the leading and trailing edges of the wing. As it passes by the wing it will be distorted, and it is this distortion that is the focus of the project. The situation is closely related to the interaction of the trailing tip vortex left behind by one blade of a helicopter rotor with other blades of the same rotor. Such helicopter blade/vortex interactions are responsible for diminished ride quality, and for increased vibration and noise.

The advantage of studying the wing rather than the rotor is that it reduces the extent of the modifications required of the computer code which will be used (one developed by a colleague at Boston University) without altering fundamentally any essential aspect of the interaction. The existing code will have to be modified to incorporate a line vortex and to properly model its convection. The challenge will be to devise a scheme to handle the distortion of the wake as it passes by the wing and interacts with the wake generated by the wing.

Computer code modifications and initial computations will be carried out at Boston University and if need be continued at NASA Ames. (Similar computers are available at both sites.) The work will be completed and written up during my second stay at Ames next summer.

ORIGINAL PAGE IS
OF POOR QUALITY

Botany Facility Feasibility Study
For Fairchild Leasecraft Freeflyer Platform

Dennis Westlake

Southwestern College Chula Vista, Calif.

The purpose of this research was to examine the critical parameters controlling the feasibility of a plant growth facility supported as a secondary payload for the Leasecraft platform. The present Plant Growth Units (PGU) and the proposed European Space Agency (ESA) Botany Facility for Europe's Free Flying, Retrievable Carrier (EURECA) were studied for possible technology applications and insight. A detailed report, describing the details of the study is available upon request.

The Leasecraft platform is Fairchild's Multimission Modular Spacecraft (MMS) adaptation for space commercialization venture. Estimated launch dates are late 1987 and mid 1988. The secondary payload specifications are listed below.

24 cubic feet
1000 Kg
1000 watts (maximum continuous)
Closed loop system (negligible venting)
6 month service intervals
Cost: 0.5 to 1.0 million dollars/month

Leasecraft Primary Payloads were studied to evaluate impact on heat dissipation capabilities of a botany facility. A typical low earth orbit was modeled and energy fluxes for varying attitudes were calculated. A "target" power range of 250 watts was proven to be feasible within a radiative surface temperature of 30 to 40 °C.

Major requirements for a closed-loop life support system for longterm plant growth were divided into the following categories:

Power Summary

Lighting	56 watts
Life Support System	120 watts
Image Collection and Control Systems	50 watts
Total	226 watts

The plant growth chamber design included two separate volumes with alternating, 12-hour day and night cycles to effect a continuous light and heat load througout the orbit. Estimated volume was 2.5 Ft^3.

The design estimate includes two banks of high temperature flourescent lamps, 22.5 watts of thermoelectric power to handle the plant's latent heat load, and 45 watts allocated for water separation and recovery. A finite difference computer simulation was employed to examine: transient dormant phase, transient heating phase, and power vs radiator surface temperature for steady state orbital heating. These data were calculated for two different radiator masses and viewing directions.

ORIGINAL PAGE IS
OF POOR QUALITY

Figure 3, included in this abstract, is a graph of 250 watts heating dissipation during transient phases for both radiators and both sun-viewing (X_s) and Z axis viewing directions. Initial temperatures were 252° K, the value approached by the dormant phase radiators following 7 or 8 orbits, at the end (or begining) of an orbit.

The Z-axis radiators approached a constant steady state value of near 5.7° C. This is the "best case" model, requiring the lowest surface temperature to radiate the heating load of 250 watts. This direction is non sun-viewing, "seeing" only deep space, Earth's infrared radiation, and Earth's albedo.

The sun-viewing radiators exhibit a fast temperature rise during the sunlight portion of their orbits, approaching a cyclic steady state behavior close to the end of the fourth orbit. The significant phenomenon here is this short orbital time necessary for the surface to increase significantly. One possible conclusion is to design for sun-viewing; although this is a conservative approach. If the heat exchange is designed for the lower temperature off-sun viewing, a very short period of direct sun exposure could easily overload the system's capacity.

The program employed for this study entitled, "Simplified Shuttle Payload Thermal Analyzer"(SSPTA), was developed by Arthur D. Little, Inc., for NASA Goddard Space Flight Center, November 1977 and revised September 1979. The author received extremely valuable direction and supervision from Scott Maa (RFD) of ARC, who made possible the program transfer to the Life Sciences VAX system in building 240-A.

The Transient Thermal Analyzer program solves a set of non-linear energy balance equations by a modified Gauss-Seidel technique using Newton-Raphson iterative procedure. Many different solution techniques and convergence criterion can be explored with this finite difference scheme.

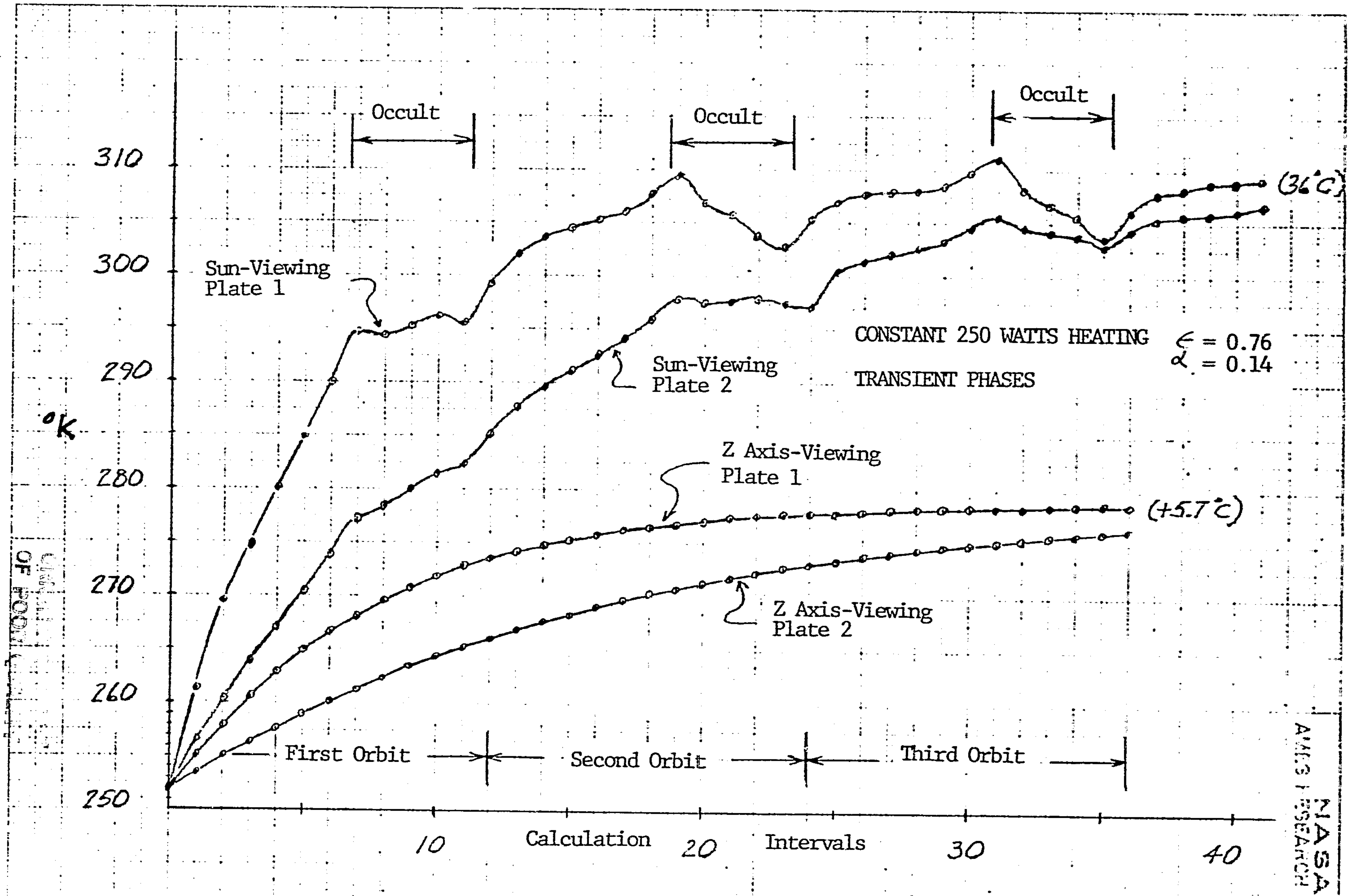

Figure 3 - Required Surface Temperature
vs Orbit Duration-250 Watts

NASA
AMES RESEARCH CENTER

Data Compression Studies for the Numerical Aerodynamics Simulator

Nicholas Weyland

Department of Computer Science

Montana State University

Bozeman, Montana 59717

The Numerical Aerodynamics Simulator (NAS) Processing System Network (NPSN) is a proposed computation resource being designed at the Ames Research Center. It will be capable of handling large computational fluid dynamics (CFD) problems. Files on the NPSN will be quite large, up to 400 MB in the initial operating configuration. With such a large amount of potential traffic it is clear that any reduction in the size of files could have the potential of increasing throughput. This summer I have researched data compression as it affects the NPSN and have proposed the design and testing of a file compression algorithm for compressing the result files or solution set files generated by solving CFD problems. These solution files are among the largest files on the NPSN. I have determined by numerical experiments that they are capable, using the proposed algorithm, of being compressed by 50% with a reasonable amount of processing overhead. This algorithm will also compress the grid files of the NPSN. This will have a significant effect on the throughput and hence productivity of the NPSN.

I will not go into the details of the proposed algorithm but refer the reader to the final report of the author submitted August 24, 1984 to the NAS projects office.

I also have plans to continue this work during the coming academic year at Montana State University. I have obtained tapes of a solution file of a fluid flow problem involving the space shuttle and plan to use these in testing the proposed algorithm. The algorithm will be

designed, coded, tested, and benchmarked against these files.

There is also the potential for further research into the area of data compression. The NASA-Stanford-ASEE fellowship has provided me with the opportunity to consider data compression problems. The field is currently very active.

Inhibition of Motion Sickness

Jacob Zabara

Temple University
Associate Professor of Physiology/Biophysics

A question arose as to the role of inhibitory nerves in the development of motion sickness, and whether inhibitory nerves can prevent or suppress motion-induced emesis.

The primary approach towards the analysis of the neural regulation of emesis, retching and nausea is almost completely based upon excitatory systems involving the emetic center and chemoreceptor trigger zone. Often this excitation is conceived as excessive stimulation of certain receptors, such as the vestibular system which results in motion sickness. There exist extensive studies of excitatory systems in motion sickness or emesis involving latency, susceptibility, ablation of brain systems to determine essential areas for vomiting, stimulation of vomiting center, chemoreceptor trigger zone and associated regions, vestibular stimulation, visual stimulation and the presence of excitatory transmitters in the cerebrospinal fluid. This research project will present data in relation to an inhibitory system which apparently acts in conjunction with the excitatory system. Specific knowledge as to the nature of these inhibitory nerves and the identification of the stimulus parameters for activation of their receptors, could lead to successful techniques to prevent emesis, retching or nausea such as occurs in motion sickness. Motion sickness studies often involve emesis or retching as an "end point" but the excitatory system model of emetic regulation has been difficult to accommodate to mechanisms of motion sickness (Wood and Graybiel; Graybiel et al.). It may be that part of this difficulty has its origin in the presence of an inhibitory system. It has been demonstrated that autogenic-feedback training can be used to teach human subjects to suppress their own motion sickness symptoms (Cowings and Toscano). A possible explanation for this increased tolerance to motion sickness observed with autogenic-feedback training is increased inhibitory influences of higher brain structures on autonomic neural centers in the brain stem. However, the nature of operation of this inhibition remains virtually unknown. A series of investigations was initiated to identify and determine the specific properties and actions of an inhibitory system in relation to emesis, retching and nausea. There are two major goals of this research: (1) a demonstration of the existence of identifiable, inhibitory nerves preventing emesis or motion sickness and (2) the elucidation of the mechanisms of this inhibitory action. The initial research upon which this project is based, was the first to present significant evidence for, and identification of, an inhibitory pathway preventing emesis. This was based on a model of emesis produced by stimulation of gastrointestinal vagal afferents. I propose to extend the experimental model to motion sickness by analysis of emesis initiated by activation of the vestibular apparatus and the chemoreceptor trigger zone. The results of the initial research model were briefly, as follows: Emesis, preceded by retching, can be induced consistently in the dog by

appropriate electrical stimulation of the abdominal vagal afferent. Stimulation is applied usually to the dorsal or ventral branches of the vagus at the supradiaphragmatic level. Presumably this result is the consequence of generating an emetic signal in abdominal afferents which can oridinarily produce emesis by appropriate activation of their receptors. However, retching and emesis have not been reported with centripetal stimulation of the cervical vagus (Agostini et al.; DeBurgh and Evans; Evans and Murray). One possible explanation is the presence of an afferent pathway which is inhibitory to retching and emesis. Evidence supporting this explanation was obtained by stimulation of the cervical vagus simultaneously with the abdominal vagus. Stimulation of the abdominal vagus alone produces emesis or retching which is absent with stimultaneous stimulation of both the cervical and abdominal vagus nerves.

The experimental procedure involves the implantation of nerve electrodes in animals, under anesthesia (pentobarbital, 35 mg/kg IP). These nerves had previously been identified as emetic-inhibitory neurons. Now, the problem is to determine whether stimulation of these neurons will prevent or suppress motion sickness. The electrode configuration has been designed as a nerve cuff in which the electrodes are embedded in a cylinder of silicone rubber. The cylinder has been slit lengthwise so that the nerve can be inserted with the electrode array lying perpendicular to the nerve trunk. The electrodes are then tested with an impedance meter to determine whether the coupling to the nerve is functional. The relationship between frequency of stimulation and impedance is non-linear so that the voltage of stimulation may have to be changed with a change in frequency to achieve optimum activation of the neural population. The measured impedance is a function of the electrodes, nerve and connective tissue. The impedance can be modelled as a simple resistance - capacitance equivalent circuit where the resistance is about 2.2 kΩ and the capacitance about 0.50 μf. The capacitance is primary at low frequencies (about 10 Hz) and is due apparently to a double layer surrounding the electrodes. The resistance is primary at high frequencies (about 1000 Hz) and is due apparently to the nerve and connective tissue.

Therefore, this summer we have developed the basis for experimental procedures to explore the role of inhibitory nerves in motion sickness.

Theoretical and Experimental Studies of the Electronic Spectra of Some Bioflavins Adsorbed on Clay Surfaces

Yvonne Jones Aronowitz
Instructor
DeAnza Community College

Biologically significant organic molecules have been found to be readily adsorbed by clays. The amount of material adsorbed can be greatly increased by previously saturating the clay with certain inorganic cations. This property has been used by many to help explain the origin of life on earth.

My research problem for the last two summers has been to try to understand the nature and extent of the bonding in these bioorganic-clay systems. Preliminary studies were undertaken last summer to obtain the room temperature and low temperature optical spectra of riboflavin and some simple bionucleotides adsorbed on clays. Changes in the electronic spectra indicated that there was significant interaction within the system depending on the nature of the exchanged cation.

As a result of the analysis of these preliminary results, three basic topics naturally developed for this summer's investigation.

The first area of concentration represents a completion of last summer's laboratory work. It was found that the optical spectra of the cation clays change significantly with temperature. Therefore, the use of a room temperature clay spectrum as the reference background for low temperature studies introduced some error into our double beam results. An unsuccessful attempt was made to find a suitable instrument to repeat this part of the experiment. The low temperature spectra of unadsorbed cation clays were taken and these spectra will be used to correct the previous data. In order to facilitate the interpretation of theoretical results, the optical spectrum of lumiflavin adsorbed on clays was also taken.

The second area of concentration was to more rigorously analyze the line spectra collected over the last two summers. Much time was spent trying to find a way to digitize the data. Equipment in the laboratory

of Dr. Jacob Miller is being used for this purpose. A BASIC program was developed to determine transition frequencies (wavelength maxima) and transition intensities (peak height and band widths). This was done by analyzing higher derivatives of the digitized data assuming simple Gaussian shapes. Most of the digitizing will be completed by the end of summer and the software program will be further developed to include other line shapes and spectrum stripping capabilities.

The final area of concentration was to calculate the nature and extent of the bonding non-bonding interaction by developing a theoretical model which could be used to predict the observed spectra. To accomplish this phase, theoretical calculations were initiated using a modified Iterative Extended Hückel (IEHT) program developed here at NASA. The program is being successfully run on a NASA VAX/VMS computer. Because of the limitations of the VAX storage, studies have been limited to simple flavin type molecules and their geometric isomers. During the academic year, some minor modifications will be made in the program in order to run it on the larger Cray computer here at NASA. When this has been accomplished, calculations will be made on the composite flavin-clay systems.

Discussions with Dr. James Lawless about future collaborative efforts have been held and have resulted in my applying for admission into the Ames Associate Program.

2ND-YEAR FELLOWS

Broadband (Optical, Infrared, and Radio) Observations of Quasars and Active Galaxies

Thomas J. Balonek

Williams College
Visiting Assistant Professor of Astronomy

The physical processes by which quasars and active galaxies produce their enormous amounts of energy remains an important unanswered astronomical question. Quasars, the most distant and luminous objects in the Universe, emit electromagnetic radiation over a wide frequency range - from radio to gamma ray energies. The relationship between the emission mechanisms and emitting regions throughout this wide range of frequencies is still not completely understood.

To investigate the energy production, transport, and emission processes which are responsible for the prodigious amounts of observed broadband radiation, I organized a program in 1982 to observe a sample of 15 quasars and active galaxies at optical, infrared, and radio wavelengths. Simultaneous observations are necessary in order to remove any effect that the time variability of the objects would have on the broadband frequency dependent intensity distribution. One to two week observing sessions were conducted at nine epochs during the past two years at eight frequencies in the optical (UBVRI) - near infrared (JHK) region of the electromagnetic spectrum, and at four radio wavelengths (3mm-6cm). The multi-epoch broadband observations will permit us to follow the evolution of outbursts, and to compare these results with theoretical predictions.

In addition to measurements of the total intensity at many frequencies, we also observed the polarization characteristics (linearly polarized flux density and position angle) at optical and near infrared frequencies. By following the time and frequency dependent changes in the source polarization, we can probe the magnetic field structure of the emitting volumes. From our results, we can address problems such as: Is there one or multiple emitting region(s) responsible for the optical-near infrared radiation; Are these regions physically related to the far infrared-radio emitting region; Do the emitting volumes change with time; and Is the magnetic field structure time or spatially dependent?

During the summer 1983, I developed a computer program to calibrate and reduce the optical data. Using this program during the past year, we completed reduction of the entire optical frequency data base. I presented preliminary results from this work at the January 1984 meeting of the American Astronomical Society. I spent the first half of this summer completing reduction of the radio data base, while a graduate student a the University of New Mexico finished reduction of the infrared data.

M. Werner and T. Roellig (my NASA-Ames colleagues for the NASA-ASEE program) have made measurements of a sample of quasars at eight infrared-microwave frequencies at several epochs. Several observations were made close in time to the optical-radio observations which my group has obtained. During the last part of the summer, I have begun analysis of the combined multi-frequency data base of the total flux density spectrum for several quasars.

One of the most interesting sources which we have studied is the BL Lacertae type quasar OJ287 (the 287th source in the Jth section of the Ohio survey of radio sources!). In January 1983, this object underwent its strongest outburst in a decade - at radio as well as at optical wavelengths (Fig. 1). Our nine consecutive nightly observations in January 1983 indicate that during the rise to and decay from maximum intensity the spectral shape (intensity as a function of frequency) at optical wavelenghts did not change (Fig. 2). Within the accuracy of our observations, we cannot detect any change in the optical spectral shape between January and May 1983, despite a factor of more than three change in the total intensity (Fig. 3). These results indicate that the energy distribution of radiating particles which produce the optical emission has remained the same throughout this period of activity.

There is some evidence that the spectrum is flatter at infrared wavelengths than at optical, which would be consistent with trends seen by previous investigators (Fig. 4). Combining these results of the spectral shape with the polarization variations observed in the January outburst (in which the polarization position angle and intensity were observed to change with time and frequency; Fig. 5), we have begun to model this outburst in terms of a two component source. In this model, two physically independent regions in the quasar are responsible for the observed intensity and polarization variations. By allowing these two components to vary independently, we can reproduce the observed fluctuations.

Most of my time at NASA-Ames the past two summers has been spent performing reduction of the large data base which we have acquired from this ambitious observing program. During the next year, I plan to continue collaborating with Werner and Roellig on the analysis of several quasars. Specificaly, we will be searching for statistical correlations between the multitude of variables (source intensity, spectral shape, fractional polarization, polarization position angle) as functions of time, frequency, and other variables. We will also be studying the broadband spectra and evolution of each of the sources in our sample. Preliminary analysis indicates that outbursts seen at optical wavelengths can be seen at later times at far infrared and submillimeter wavelengths, indicating a common emitting volume and mechanism. The data obtained by Werner and Roellig will be important in this analysis. Further coordinating observations of this sample of quasars may be scheduled if the results from our present study continue to prove promising.

OF POOR QUALITY

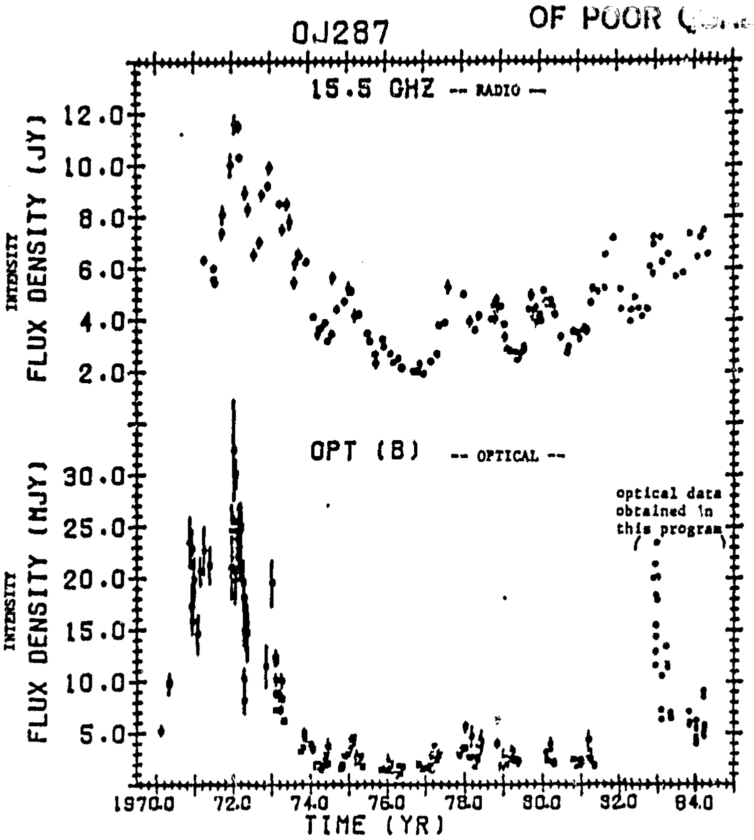

FIGURE 1

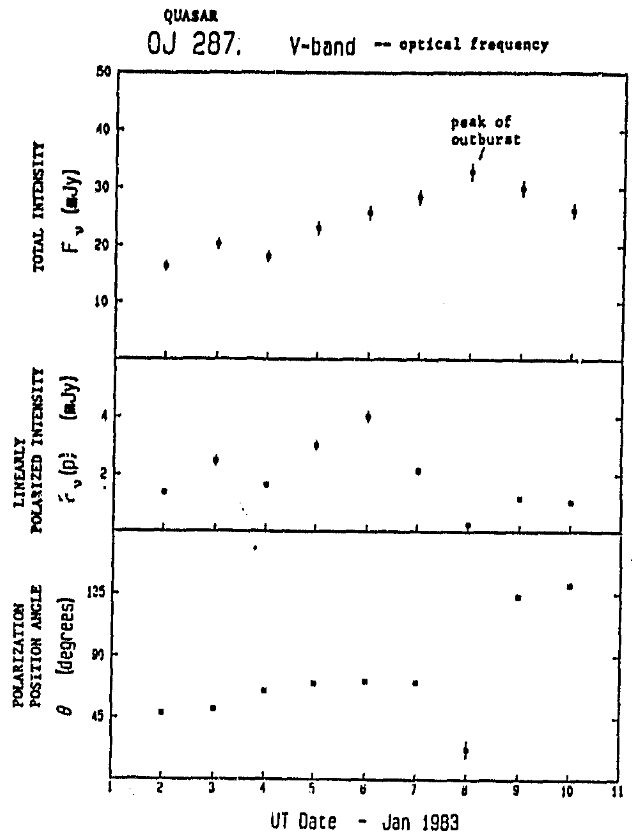

FIGURE 5

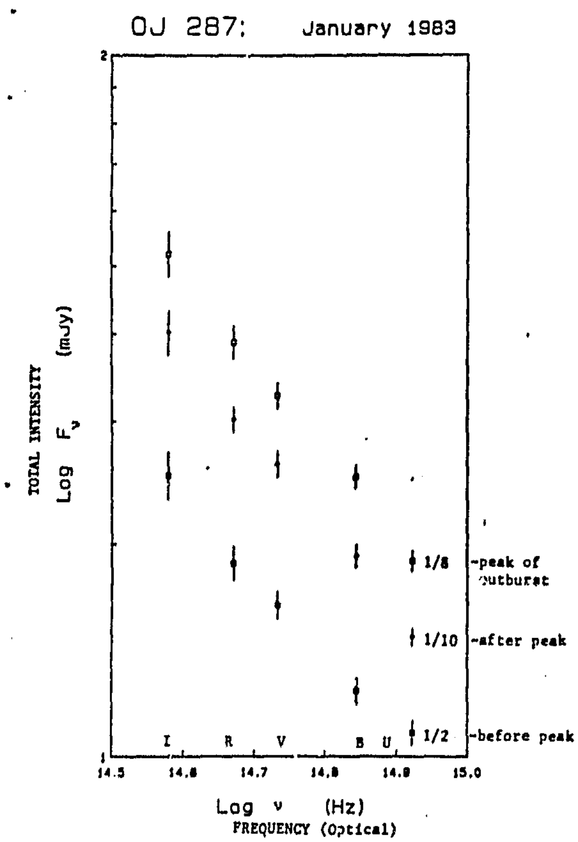

FIGURE 2

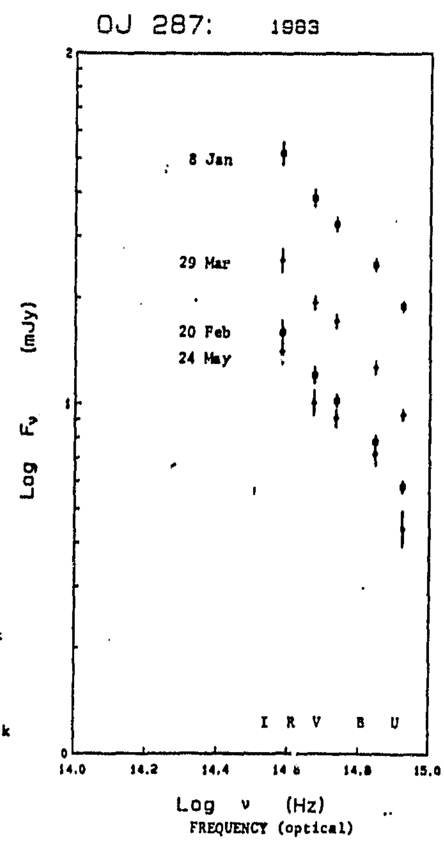

FIGURE 3

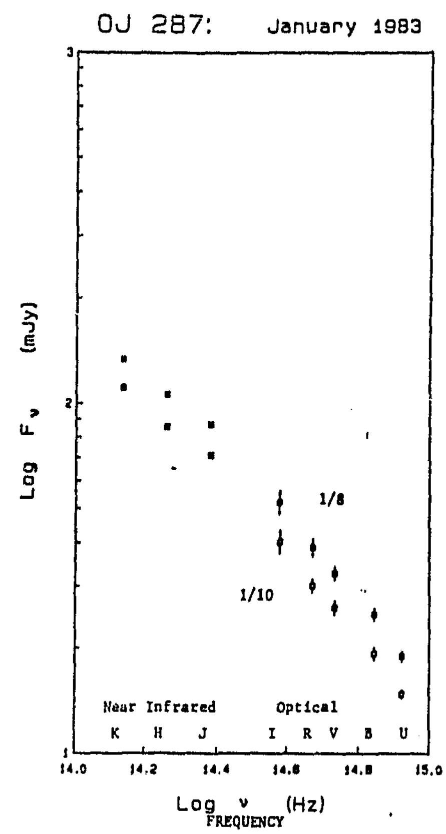

FIGURE 4

Ann B. Cox, Ph.D.
Colorado State University
Final Report, NASA-ASEE Stanford Summer Program, 1984

Preprint of article to appear in the Proceedings of the 25th Plenary Meeting of the Committee on Space Research (COSPAR), June-July 1984, to be published by Pergamon Press in Advances in Space Research 1984.

QUANTITATION OF HEAVY-ION DAMAGE TO THE MAMMALIAN BRAIN: SOME PRELIMINARY FINDINGS

A. B. Cox* and L. M. Kraft**

*Department of Rad. ·ogy and Radiation Biology, Colorado State University, Fort Co. ·ns, CO 80523 U.S.A., **Biomedical Research Division, NASA Ames Research Center, Moffett Field, CA 94035 U.S.A.

ABSTRACT

Histological preparations of brains from rabbits and mice exposed to different doses of various HZE particles or to low-LET photons have been subjected to preliminary quantitation of radiation-induced morphometric changes. Computer assisted measurements of several brain structures and cell types have been made using the KONTRON Automated Interactive Measurement System (IBAS, Carl Zeiss, Inc., Thornwood, N.Y. 10594 U.S.A.). New Zealand white rabbits irradiated at ~6 weeks of age were euthanatized 6.5-25 months after exposure to ^{60}Co gamma photons (LET_{∞} = ~0.3 keV/μm), ^{20}Ne particles (LET_{∞} = 35 ± 3 keV/μm) or ^{40}Ar particles (LET_{∞} = 90 ± 5 keV/μm). Measurements of stained sections of the olfactory bulbs of those animals indicate that the mean size (volume) of olfactory glomeruli is reduced in a dose-dependent (and perhaps an LET-dependent) manner) as soon as 6.5 months after irradiation. Differences between mean volumes of additional structures have been noted when histological preparations of control mouse brains were compared with irradiated specimens. Quantitation of intermediate and late changes in nervous (and other) tissues exposed to low- and high-LET radiations will improve our ability to predict late effects in tissues of astronauts and others exposed to the radiation hazards of the space environment.

INTRODUCTION

For several years we have been studying late effects of particulate radiations in mammalian tissues, including the brains, of rodents and lagomorphs /1,2,3,4/. Our published results primarily are descriptive of radiation-induced damage /1/, and until recently quantitation has been based largely either on subjective scoring of brain damage /2,4/ or on labor-intensive measurements such as cell counts (e.g. counts of necrotic neurons and neuroglial cells, etc.) /1,3/. Included among our research goals are accurate determinations of the relative biological effectiveness (RBE) of particulate radiations typical or representative of those to which astronauts have been and will be exposed in the space environment. Ground-based experiments have been performed on animal models using the BEVALAC of the Lawrence Berkeley Laboratory (University of California) as the source of high linear energy transfer (LET) radiations. While descriptive and subjective evaluations of radiation damage to nervous tissues have been fruitful in the past (e.g. /1,2,3,4/), objective large scale quantitation of such damage promises to provide additional vaulable data for calculations of RBE values. The KONTRON Automated Image Analysis System (IBAS) provides a means by which that quantitation can be achieved.

Late radiation-induced changes in mammalian tissues have been characterized in a number of different ways (e.g. /1,2,3,4,5,6,7,8/), but only recently has it become feasible to quantify pathological damage and morpho-physiologic alterations accurately in large numbers of histological specimens. The development of computer-assisted automated image analysis systems has given investigators the opportunity not only to measure areas and volumes of structures in histological preparations, but also to determine degrees of gross pathological changes by rapid scanning of specimens with quantitation of, e.g., optical density differences between regions. Until this technology was developed, only tedious and relatively inaccurate measurements of microscopic structures could be made, and the data obtained thereby tended to be sparse. Now systems such as the IBAS allow image enhancement, computer controlled scanning, large numbers of accurate area and volume measurements, etc., to be attained. Over the past 6-8 years, the authors independently have accumulated histological specimens of control and irradiated rabbit and mouse brains /1,2,3,4/ in anticipation of access to a system such as the IBAS, and preliminary data obtained using the system indicate that radiation effects can be quantified in such tissues.

ORIGINAL PAGE IS
OF POOR QUALITY

/ 8 3.3.

(2)

ORIGINAL PAGE IS OF POOR QUALITY

METHODOLOGY

Rabbit Irradiations

New Zealand white rabbits (Oryctolagus cuniculus) were exposed to single acute doses of ionizing radiation when they were ~6 weeks old. The 2.5 cm diameter beam entered the right eye and emerged through the left in each case. A portion of the forebrain (including both olfactory bulbs) was irradiated as well. The radiations employed were 1) ^{60}Co gamma photons (LET_{∞} = ~0.3 keV/μm), 2) 365 MeV ^{20}Ne ions (Bragg plateau LET_{∞} = 35 $\pm$ 3 keV/μm) and 3) 525 MeV ^{40}Ar ions (Bragg plateau LET_{∞} = 90 $\pm$ 5 keV/μm). Particulate radiation exposures were performed at the BEVALAC facility of the Lawrence Berkeley Laboratory (University of California). Further details of the rabbit irradiation procedures and of the standard histological procedures used to prepare brain tissues for evaluation may be found in references 2,4,6,7 and 8.

Mouse Irradiations

Mouse brains were kindly contributed by Dr. R.J.M. Fry and his associates from representative groups that had been irradiated at doses below 10 Gray in the course of a study on high-LET radiation carcinogenesis /5/. All mice were perfused via the heart with a paraformaldehyde-glutaraldehyde fixative in sodium cacodylate buffer. Ten-μm thick serial sections were cut from brains, including olfactory bulbs, in the coronal plane and stained with hematoxylin and eosin.

Automated Interactive Image Analysis

A Zeiss Ultraphot photomicroscope was used for all tissue observations and measurements. A television camera mounted on the microscope was connected to a video monitor and computer. These in turn were interfaced with a second video screen and a second computer. By means of a cursor and a magnetized tablet, parts of stored images were outlined, and the computer determined the areas within those outlines based on calibration factors preset by the investigators. Area values were stored on magnetic disks for subsequent statistical evaluations.

Measurements of Rabbit Olfactory Glomeruli

A sagittal section through the olfactory bulb of a given rabbit brain specimen was located on each slide to be evaluated. Code numbers were assigned to each set of measurements to be performed on each field. All measurements were made of fields magnified 300 times, and a single preset scale factor used for all area determinations was entered into the computer before any evaluations were made. A field including several olfactory glomeruli was found, and the focused image was entered into computer #1. The image was held on the screen and enhanced to improve contrast. Interfacing between the enhanced image and the magnetic tablet allowed each olfactory glomerular area to be outlined; outlines appeared as overlays on monitor #1. When all glomeruli within a given field were outlined, their areas (in μm^2) were determined by the computer and results were stored on magnetic disks. When adequate data had been accumulated, information from each animal and from each group of animals (based on type of radiation received, dose, and post-irradiation time) was evaluated using additional IBAS statistical evaluation programs.

Measurements of Structures in Mouse Brains

Several attempts were made to measure olfactory glomeruli in the mice, but it soon became obvious that the delineation of representative structures was not as distinct in the mouse as it was in the rabbit. Therefore, since serial sections were available, volumes of well-defined zones in the bulb were determined, e.g. outer plexiform layer, granular layer, mitral and inner plexiform layers. Data from these measurements will be available at a later time. For the moment, suffice it to say that provocative results, that require confirmation, have been obtained.

RESULTS AND DISCUSSION

Radiation-induced Changes in Rabbit Olfactory Glomeruli

The olfactory bulbs of rodents and lagomorphs are relatively large structures consisting of regions which can be distinguished in stained histological preparations. The glomeruli comprise a well-defined layer of "spherical" structures in the rabbit. Sensory input from the olfactory mucosa travels via processes of neuroepithelial cells which synapse in the glomeruli of the olfactory bulb with processes of tufted and mitral cells /9/. Measurements of individual glomerular areas on 5- to 10-μm thick sections provide an indication of glomerular volumes. Since all rabbit brain sections examined were cut from similar levels /4/, comparisons between experimental and control groups were made after mean glomerular areas were obtained for each rabbit using the IBAS.

Preliminary measurements with the IBAS were made of sectioned olfactory glomeruli from rabbits which had received relatively high doses of radiation 6.5-25 months before they were euthanatized. Mean glomerular areas for control animals were greater than those found for all irradiated rabbits measured (see Table). Most measurements were made on tissues obtained 17-25 months after irradiation, but the mean glomerular areas ascertained for two groups of argon ion irradiated animals at 6.5 or 7 months post exposure also were low, implying that shrinkage of olfactory glomeruli may be a relatively early effect from which brain tissue cannot recover after the doses (fluxes) employed.

TABLE Mean Areas of Olfactory Glomeruli from Rabbits Exposed to Radiations of Different Linear Energy Transfer (LET)

Type of Radiation	LET_{∞} (keV/μm)	Number of Rabbits	Dose (Gray)	Months at Risk (mean)	Mean Glomerular Area ($\mu m^2 \times 10^3$)
Control	——	4	0	10	8.5
^{60}Co gamma photons	0.3	3	10	24	6.1
		3	20	18	3.8
^{20}Ne ions	35 ± 3	4	10-15	16	4.8
^{40}Ar ions	90 ± 5	6	7-9	16	5.2
		4	9-12	7	5.5

The data were analyzed statistically in two different ways. All mean glomerular area values for irradiated animals were significantly different from mean values for control rabbits based on t-tests. In addition, Mann-Whitney U tests were performed to compare median values of glomerular areas for irradiated animals with those for controls. All irradiated specimens measured yielded median glomerular area values which were significantly lower than controls. The dramatic reduction in size of olfactory glomeruli from irradiated rabbits could stem from one or more factors. Loss of neurons from the olfactory bulb is possible, especially at such long intervals after irradiation. Reduced numbers of neuroepithelial cells and concommitant diminution of olfactory input might have led to the shrinkage of sensory processing structures in the forebrain, but in the case of the irradiated rabbits under discussion, a relatively small proportion of the olfactory epithelium was exposed to ionizing radiation in each subject. Even if no neurons were lost, their ability to maintain pre-irradiation synaptic relationships at an optimal level might have been diminished by irradiation, and this in turn could have led to reduced function and partial atrophy. It is unclear whether the observed effect is due to the response of the glomeruli to direct damage or to secondary neuronal/glial effects. A final factor could be early, intermediate and late radiation effects on the microvasculature. Quantitation of such damage will be achieved most accurately by measuring and/or counting the appropriate vessels in the perfused specimens of the irradiated mouse brains on hand.

In conclusion, the radiations of high LET seemed to cause earlier and more dramatic shrinkage of olfactory glomeruli in exposed rabbit brains than did comparable doses of ^{60}Co gamma photons. Of course, more dose groups from all experiments must be examined using tissues from animals euthanatized at earlier and much later post-irradiation times before final statements can be made about the values for the relative biological effectiveness of heavy ions pertinent to space biology. Nonetheless, the data shown in the Table do allow us to suggest that radiation effects may be measured in histological preparations of brain tissues, and that by means of tools such as IBAS, quantitation of radiation effects in tissues previously thought too difficult to study is now a realistic goal.

ACKNOWLEDGEMENTS

This research was supported by grants NGR 06-002-128 and NSG 9045 from the National Aeronautics and Space Administration (NASA) and AG 00005 from the National Institute on Aging of the National Institutes of Health. Additional support was provided by a contract granted to the Lawrence Berkeley Laboratory by the Department of Energy. The research reported herein was performed in the laboratory of the second author while the first author was a Stanford University NASA-ASEE (American Society of Engineering Education) visiting faculty fellow at NASA Ames Research Center.

(4)

F 3.3.3.

ORIGINAL PAGE IS
OF POOR QUALITY

REFERENCES

1. L.M. Kraft, M.A. Kelly, J.E. Johnson, Jr., E.V. Benton, R.P. Henke, R. Cassou, W. Haymaker, D.E. Philpott, F.S. Vogel and W. Zeman, Effects of high-LET neon (^{20}Ne) particle radiation on the brain, eyes and other head structures of the pocket mouse: a histological study, Int. J. Radiat. Biol. 35, 33 (1979)

2. J.T. Lett, A.B. Cox, P.C. Keng, A.C. Lee, C.H. Su and D.S. Bergtold, Late degeneration in rabbit tissues after irradiation by heavy ions, Life Sciences and Space Research XVIII, 131 (1980)

3. L.M. Kraft, F.E. D'Amelio and E.V. Benton, HZE particle effects in the mammalian brain; relevance to manned space flight, in: Biological and Medical Research with Accelerated Heavy Ions at the BEVALAC, 1977-1980, LBL-11220, UC-48, 287, Lawrence Berkeley Laboratory, Berkeley, California (November 1980).

4. A.B. Cox, P.C. Keng, A.C. Lee and J.T. Lett, Effects of heavy ions on rabbit tissues: damage to the forebrain, Int. J. Radiat. Biol. 42, 355 (1982).

5. R.J.M. Fry, P. Powers-Risius, E.L. Alpen, E.J. Ainsworth and R.L. Ullrich, High-LET radiation carcinogenesis, Adv. Space Res. 3, #8, 241 (1983)

6. P.C. Keng and J.T. Lett, Effects of heavy ions on rabbit tissues: loss of electroretinogram and DNA repair in retinal photoreceptor cells, Int. J. Radiat. Biol., 39, 655 (1981)

7. A.B. Cox, P.C. Keng, N.L. Glass and J.T. Lett, Effects of heavy ions on rabbit tissues: alopecia, Int. J. Radiat. Biol., 40, 645 (1981)

8. P.C. Keng, A.C. Lee, A.B. Cox, D.S. Bergtold and J.T. Lett, Effects of heavy ions on rabbit tissues: cataractogenesis, Int. J. Radiat. Biol., 41, 127 (1982).

9. P.F.A. Martinez Martinez, Neuroanatomy. Development and Structure of the Central Nervous System, W. B. Saunders Company, Philadelphia, 1982.

THE USE OF ADVANCED COMPUTER TECHNIQUES IN THE CARDIOVASCULAR RESEARCH LABORATORY

BY: JOHN S. DAPONTE
COMPUTER SCIENCE DEPARTMENT
SOUTHERN CONNECTICUT STATE UNIVERSITY
501 CRESENT ST.
NEW HAVEN CT. 06515

My assignment in the CARDIOVASCULAR RESEARCH LABORATORY at NASA/AMES this past summer involved the use of advanced computer techniques in three applications. The first application was the use of a sophisticated signal processing software package named SIG to perform FOUIER ANALYSIS on data obtained from the COSMOS 1514 PRIMATE SPACE FLIGHT. The second application was the use of the BMDP, statistical software package, for data reduction of experimental results obtained from water immersion studies conducted at NASA/AMES. The third application was the design, coding and implementation of a program to calculate and plot various phisiological parameters resulting from ultra sound crystal implanted in RHESUS MONKEYS.

The object of the signal processing effort was to calculate VASCULAR IMPEDANCE as the transfer function of carotid arterial pressure and flow. After investigating various aspects of SIG the following general procedure was developed:

1. Transfer uncalibrated pressure and flow data from the PDP 11/34, in the Cardiovascular Lab, to the VAX 780, in the computational center, via the cardiovascular network.

2. Use SIG to read the VAX data files into the SIG data base.

3. Apply calibration slope and intercept parameters by using the CMULTIPLY and CADD SIG functions for both pressure and volume time signals. These factors are currently available for flow and should be available for pressure in the near future.

4. Window time signals with a FULL HAMMING WINDOW as supplied in SIG.

5. Transform signals into the frequency domain using the FAST FOURIER TRANSFORM (FFT) function of SIG. The windowing of step 4 will produce a frequency spectrum in which a larger portion of the total energy of the signal is in the main lobe with side lobes that decrease rapidly in energy as frequency increases.

6. Divide the frequency spectrum of the pressure by the frequency spectrum of the flow yielding the frequency spectrum of the VASCULAR IMPEDANCE.

7. The amplitude of the VASCULAR IMPEDANCE can easily be plotted using

the FSQUICKPLOT routine of SIG. If a phase plot is desired then the FSPLOT function, with changes in various defaults, should be used. Typing the number 6 in response to the prompt after each SIG plot provides for rescaling.

A typical SIG program for producing VASCULAR IMPEDANCE would be as follows:

```
TSREAD        1      E270CAP.329
TSREAD        2      E270CAF.329
CMULTIPLY     2 3    22.389567
CADD          3 3    -0.561142
CMULTIPLY     3 3    3.19
CMULTIPLY     1 4    M
CADD          4 4    B
FFT           4 5    0
FFT           3 6    0
DIU           5 6    7
FSQUICKPLOT   7
```

Where E270CAP.329 and E270CAF.329 are the VAX file names for the uncalibrated pressure and flow respectively. The values 22.389567, -0.561142 and 3.19 are used to calibrate and convert the flow signals, while M and B are calibration factors (to be supplied) for pressure.

The objective of the statistical applications was to use analysis of variance to determine if there was a significant difference among various groups of monkeys before water immersion, during immersion, and after immersion. Groups consisted of conscious, tranquilized and anesthetized monkeys. The P2V routine of BMDP was identified as providing the most applicable results. This type of experiment is called a REPEATED-MEASURES DESIGN wth one grouping factor and one within factor. BMDP programs were written for various dependent variables and results have been provided.

A sample BMDP control file used to direct P2V is as follows:

```
/PROBLEM TITLE IS 'SODIUM EXCRETION DATA'.
/INPUT VARIABLES ARE 4.
     FORMAT IS '(F1.0, 3F5.2)'.
     FILE IS NAEXCR.DAT.
/VARIABLE NAMES ARE GROUP, NA1, NA2, NA3.
/DESIGN DEPENDENT ARE 2 TO 4.
     LEVEL IS 3.
     GROUPING IS GROUP.
     NAME IS TIME.
/END
```

The primary object of the dimension processing program is to calculate a large number of CARDIOVASCULAR PARAMETERS such as HEART RATE, AORTIC PRESSURE, LEFT VENTRICULAR PRESSURE, VENTRICULAR WALL THICKNESS, AORTIC FLOW, MAXIMUM and MINIMUM LEFT VENTRICULAR VOLUME using spherical and elliptical geometric models. Another objective was to produce PV LOOPS. Thus the dimension processing program outputs a file that contains intructions and data that can plot PV LOOPS using the TELLAGRAF software package. This program also con-

tains a file that can be used to transfer data to the SIG software package so that VASCULAR IMPEDANCE can be obtained. Another program should be written in the future to calculate the STROKE WORK as the area of the PV LOOP. By comparing these loop areas during baseline conditions versus various experimental interventions, the amount of work expended during the different CARDIAC CYCLES can be compared.

A system flow chart of the dimension processing program follows.

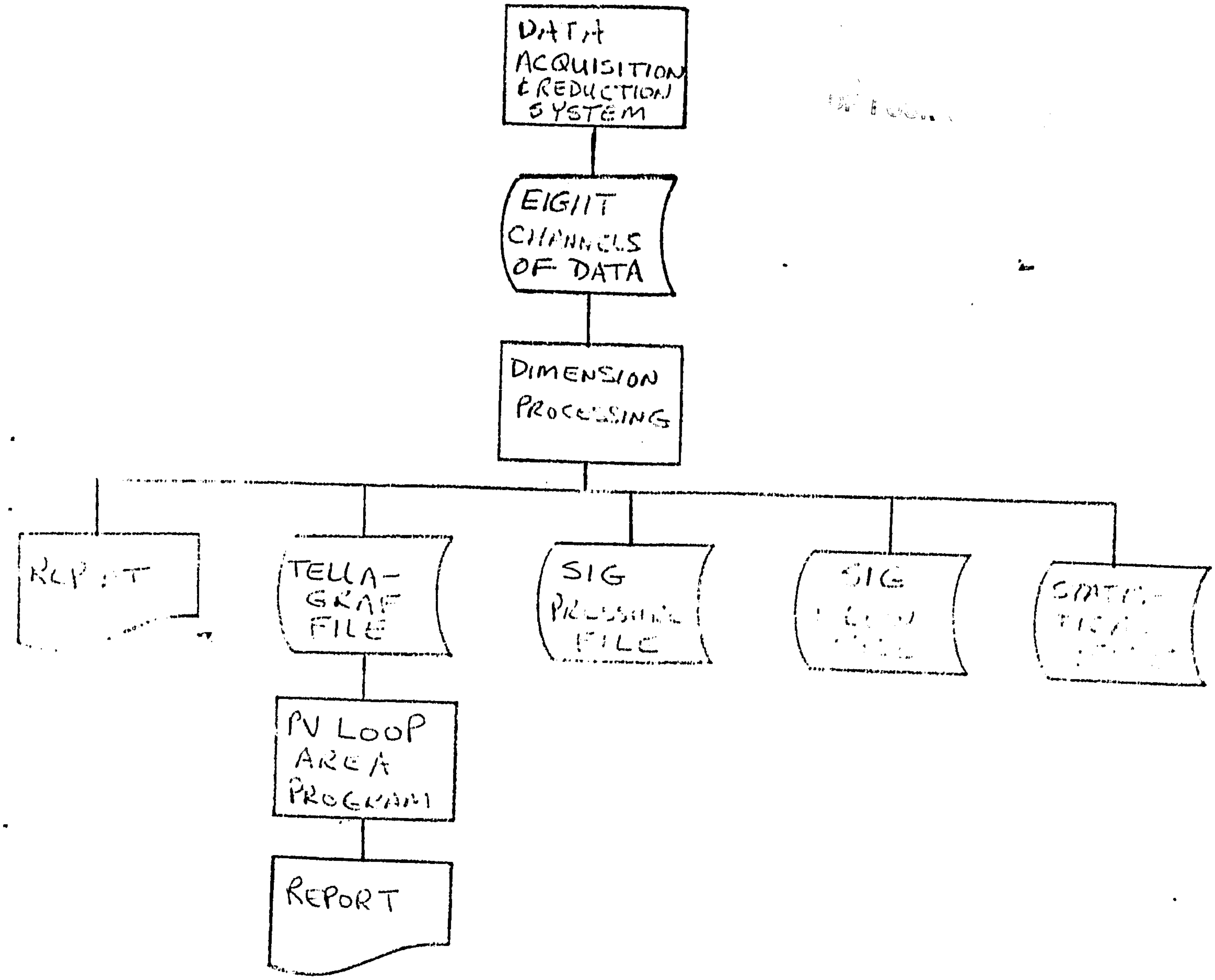

SIGNAL DETECTION IN THE SEARCH FOR EXTRATERRESTRIAL INTELLIGENCE (SETI)

Stanley R. Deans
University of South Florida
Professor of Physics

Scientists at NASA-Ames Research Center, Stanford University, and the Jet Propulsion Laboratory are carrying out a five-year research and development program to develop powerful instrumentation to attempt detection of signals generated by other intelligent beings, if such signals exist. My contribution to this effort is in the software development for the signal detection system ultimately to be used for extraterrestrial intelligence signal searches. My work on this project can be divided into three related topics. These topics and associated progress reports are listed below.

A. Development of new signal detection algorithms

Adaptation of the Radon transform[1] to the signal detection problem was accomplished during the summer of 1983. Further refinement of the technique continued during the following academic year at the University of South Florida, Tampa. The remaining part of this work is closely related to the evaluation of detection algorithms.

B. Development of methods for systematically evaluating detection strategies

An important part of evaluation and subsequent optimization involves the rapid computation of various statistical parameters and the determination of their interdependence. A considerable portion of the current summer work has been devoted to the development of efficient computational procedures and related illustrations of the important interrelationships. Samples of these results are shown in the Figures (obtained using the DISSPLA graphics package).

It should be emphasized that the major difficulty (and thus the major contribution) is the extension of existing tabulated results[2] to regions that are excessively tedious to compute due to overflow and/or underflow problems. (This is related to the very-low-probability searches that must be carried out in SETI.) It is necessary to sum hypergeometric series that contain many large terms, such as 3.87512×10^{487} The trick that makes the computations feasible is to sum the hypergeometric series in a special logarithmic mode that produces the logarithm of the desired function rather than the function itself.

C. Optimizing detection strategies

Work on optimization is just beginning. Discussions with several members of the SETI group at Ames are underway and various approaches to constrained optimization are being studied.[3,4] Further work on this and other SETI related projects will continue during the coming year when I will be on leave from the University of South Florida to accept a National Research Council (NRC) Senior Research Associateship at NASA-Ames Research Center beginning October 1, 1984.

REFERENCES

1. S. R. Deans, *The Radon Transform and Some of Its Applications*, Wiley-Interscience, New York (1983).
2. G. E. Haynam, Z. Govindarajulu, and F. C. Leone, "Tables of the cumulative non-central chi-square distribution." in *Selected Tables in Mathematical Statistics*, Vol. 1, pp. 1-78, H. L. Harter and D. B. Owen, Eds., American Mathematical Society, Providence, Rhode Island (1970).
3. D. P. Bertsekas, *Constrained Optimization*, Academic Press, New York (1982).
4. D. G. Luenberger, *Optimization by Vector Space Methods*, Wiley, New York (1969).

FIGURE CAPTIONS

Fig. 1 Chi-square density. The probability of false alarm P_{fa} is the shaded area from threshold b to ∞.

Fig. 2 Non-central chi-square density for fixed signal-to-noise ratio r and different degrees of freedom.

Fig. 3 Same as Fig. 2 with different r.

Fig. 4 Relationship between signal-to-noise ratio in decibels and the probability of missing a signal with fixed n and P_{fa}.

Fig. 1

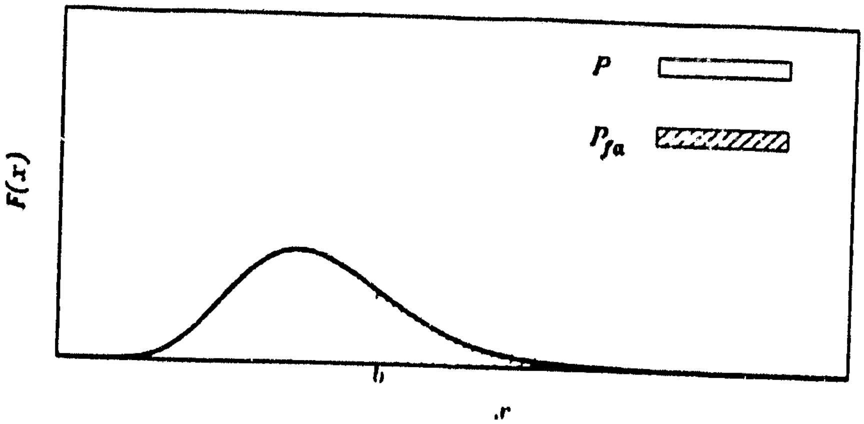

Fig. 2

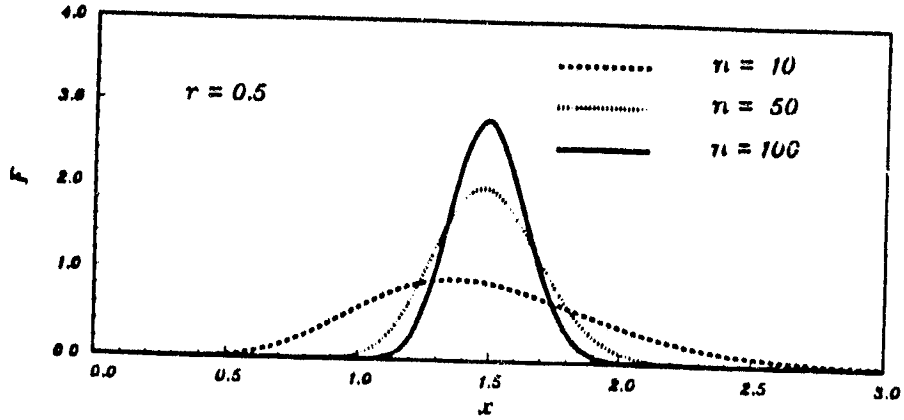

Fig. 3

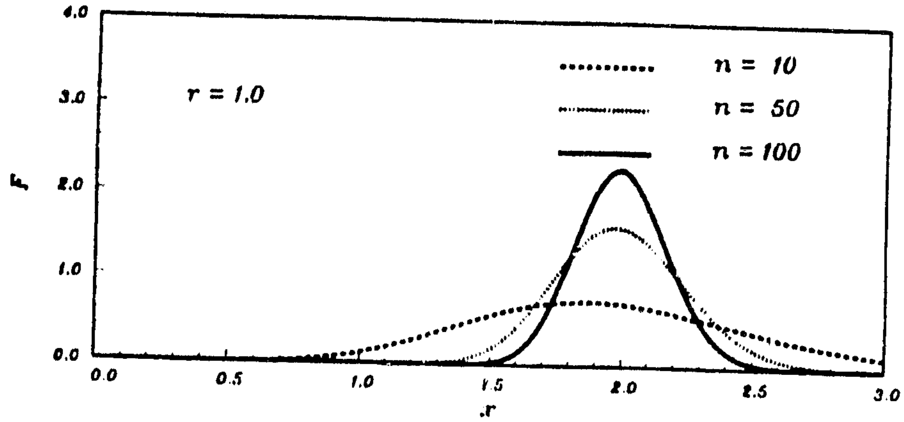

Fig. 4

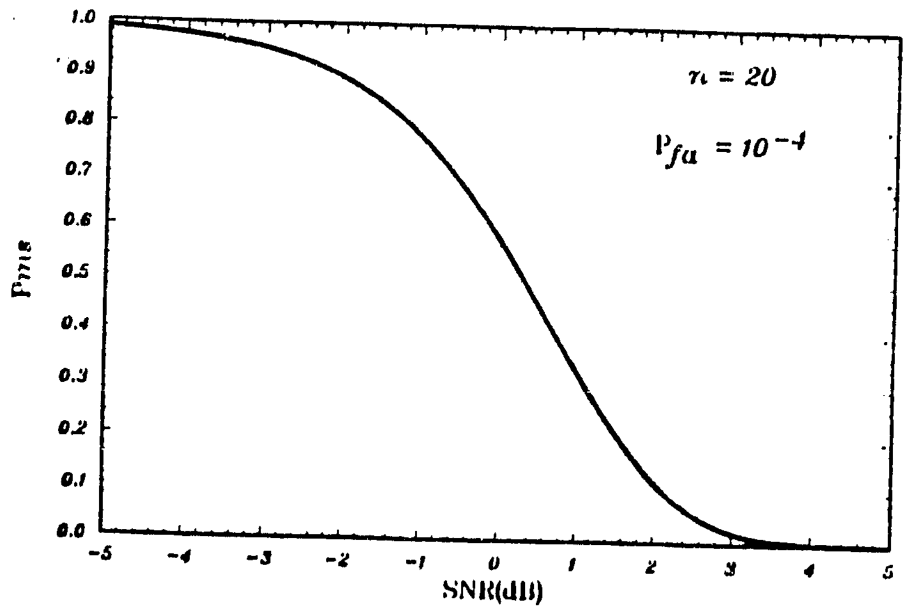

Microbiology of Hydroponically Grown Plants in CELSS (Controlled Environment Life Support Systems)

Diane Dudzinski, Ph.D.
College of Santa Fe
Professor of Biology
Chairperson, Dept. of Science/Math

Survivability of man in an extraterrestrial environment, such as a space station, for extended time may in part depend upon life support systems using higher plants to supply oxygen, potable water and contamination-free food. Such an environment on earth can be simulated by using a CELSS approach in which higher plants are grown in recirculating hydroponic and/or aeroponic chambers under controlled environment conditions. Prototype chambers have been developed and modified over the past few years at NASA/AMES in the CELSS laboratory of Robert MacElroy/Steve Schwartzkopf. During this time mechanisms for controlling indigenous microbial populations in lettuce and tomato monocultures have been modified and compared to determine relative effectiveness in reducing microbial abundance and altering species diversity within such systems.

Isolation and identification of microorganisms involved use of spread plate preparations of microbiological samples on Trypticase soy agar followed by inoculation of colony isolates into Hoffman La Rouche miniaturized and rapid microbiological systems. Samples were collected aseptically 3 times per week from plant troughs in recirculating nutrient systems. Nutrient samples were collected simultaneously with microbiological samples and were analyzed for micronutrients. Lettuce and tomato seeds were germinated between moistened filter paper and planted within the growth chambers between alcohol-washed polyurethane plugs. Prior to planting the hydroponic nutrient delivery systems were flushed with 20% sodium hypochlorite and rinsed with deionized water for a few hours. Nutrient solution was recirculated through the chamber until plant harvest at the end of 3-5 weeks. Control of microbial population density was achieved by continuous use of an on-line ultraviolet lamp emitting 245 nm, or a .22 μ bacteriological filter placed within the recirculating nutrient system. The bacteriological filter was replaced weekly.

Microbial cell densities reached 10^8 cells per ml. in control units and 10^4 cells per ml. in UV and filter treatment units. Past problems involving iron loss due to breakdown of the Hoagland nutrient solution chelator by UV treatment were overcome by weekly replacement of lost iron. Such problems were nonexistant in bacteriological filter treatment systems. Bacteriological filter units generally reached 10^6 cells per ml. prior to filter replacement. Figure 1 shows microbial cell numbers during growth of lettuce monocultures in a controlled hydroponic plant growth chamber. UV radiation and .22 μ bacteriological filter treatments reduced bacterial cell numbers by 50%. Lettuce plants were grown to maturity within 21 days as compared to 35 days in earlier experiments. Comparisons of microbial species diversity show differences between control and UV or .22 μ filter treatments, as well as between lettuce and tomato monoculture systems as appear in Figure 2. Future investigations could be directed at studying microbial community structure within other monoculture and polyculture systems and in particular at lettuce and tomato polycultures. Also of interest would be studies regarding selective seeding of naturally occurring and/or bioengineered microbes, as well as bacteriological systems modelling of indigenous and exogenous pathogenic species within such systems.

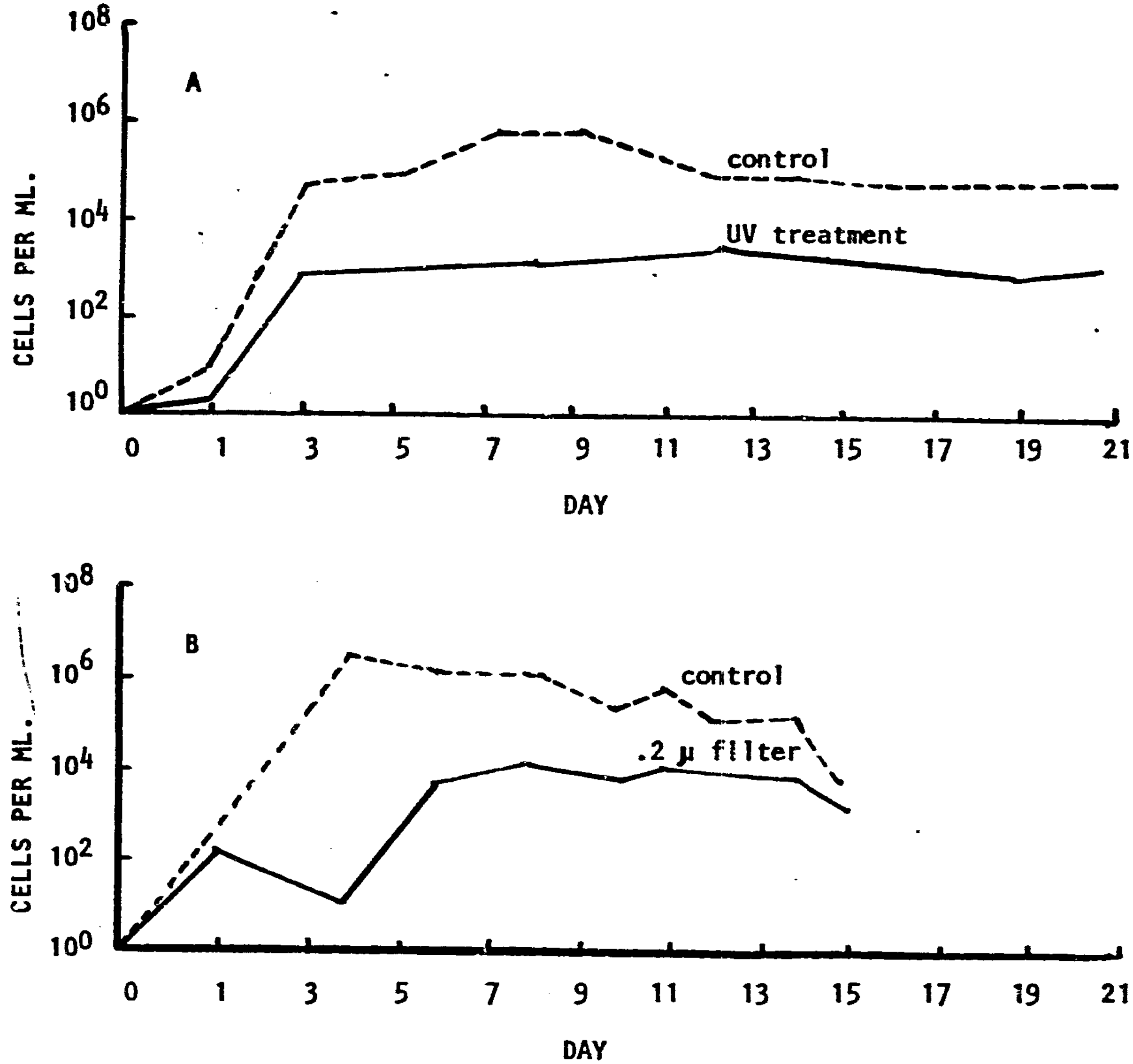

FIGURE 1 Microbial cell numbers during growth of 'Grand Rapids' lettuce (Lactuca sativa L.) in a controlled environment hydroponic chamber. UV treatment (A) and .2 µ bacteriological filter treatment (B) reduced cell numbers by 50%.

BACTERIA ISOLATED FROM TOMATO MONOCULTURE

- • Acinetobacter lwoffii
- • Acaligenes faecalis
- Group m-4f Moraxella-Like
- Group 2K-1 Pseudomonas-Like
- Pseudomonas aeruginosa
- • Pseudomonas cepacia
- • Pseudomonas fluorescens
- Pseudomonas maltophilia
- • Pseudomonas putida
- • Staphylococcus aureus

Total no. of species $(S_1) = 10$

BACTERIA ISOLATED FROM LETTUCE MONOCULTURE

- Moraxella nonliquefaciens
- Acinetobacter anitratus
- • Acinetobacter lowfii
- • Alcaligenes faecalis
- • Pseudomonas cepacia
- • Pseudomonas fluorescens
- • Pseudomonas putida
- Pseudomonas vesicularis
- Chromobacterium sp.
- Flavobacterium aquatile
- Group 5A Pseudomonas-Like
- Pseudomonas aeruginosa
- Serratia liquefaciens
- Spnaerctilus natans
- Leptothrix sp.
- Lactobacillus sp.
- • Staphylococcus aureus
- Staphylococcus epidermis
- Streptococcus faecalis

Total no. of species $(S_2) = 19$

Quotient of Similarity Calculation

$$CC = \frac{2c}{S_1 + S_2}$$

c = no. of species in common

$$CC = \frac{2(6)}{10 + 19} = \frac{12}{29} = .41 \text{ or } 41\%$$

FIGURE 2

Bacteria isolated from hydroponically grown lettuce and tomato monocultures e..hibit differences in diversity. A quotient of similarity calculation shows 41% similarity of species between the two monoculture systems.

REFERENCES

1. Buyanovsky, J. and Gale, J. 1981. Ultraviolet Radiation for Inactivation of Microorganisms in Hydroponics. Plant and Soil 60, 131-136.

2. Hammer, P. A., Tibbitts, T. W., Langhams, R. W., and McFarlane, J. C. 1978. Baseline Growth Studies of 'Grand Rapids' Lettuce in Controlled Environments. Amer. Soc. Hort. Sci. 103 (5):649-655.

3. McGuire, Jr., B. 1980. Literature Review of Human Microbes Interaction with Plants. NASA Contractor Report 166330.

CAPACITY AND CODING FOR A DIRECT-DETECTION OPTICAL FIBER CHANNEL

Mark A. Herro
Department of Electrical Engineering
University of Notre Dame
Notre Dame, IN 46556

Research Summary

ASEE Summer Faculty Fellowship Program

August 1984

Previous research on coding for direct-detection optical communications has primarily been focused on the quantum limited channel in the absence of thermal receiver noise. For uncoded systems, considerable analysis has been performed on models which include both thermal noise and an Avalanche Photo-detector (APD). In this paper we introduce a general non-additive Gaussian noise channel model which includes the effects of both quantum and thermal noise. We use this model to obtain the capacity and performance of a direct-detection optical communication system using 2^L-ary Pulse Position Modulation (PPM) and an APD. The performance is evaluated as a function of the receiver threshold setting and the PPM alphabet size.

We examine the performance of rate 1/2 Reed-Solomon (RS) coded PPM systems. The symbol size of the RS code is 2^L-1 when 2^L-ary PPM is used. The receiver operates as follows. The received voltage is compared to a predetermined threshold and if the voltage in one of the 2^L time slots in a codeword exceeds that value, a pulse is declared present; otherwise, no pulse is detected in that time slot. If only one time slot produces a pulse, the corresponding symbol is passed to the RS decoder. Two demodulating methods are considered for generating the RS code symbols when either no pulse or more than one pulse

is detected in a word. In the first method, if more than one time slot in a word contains a pulse, one of these time slots is randomly chosen to generate the code symbol. If no pulse is detected in an entire word, one of the 2^L slots is picked at random to identify the symbol. An alternate approach is to declare an erasure except when *exactly* one pulse is detected in a word time. This information is passed on to the decoder as "side information." The RS decoder then acts as an error plus erasure decoder.

The error performance of these two schemes is compared as a function of the threshold setting and the number of bits, L, in a code symbol. Previous work has shown that in the absence of thermal noise, the best threshold (in terms of minimizing the overall error probability) should be about 1 photon. However, when thermal noise is present, our channel model predicts that the optimum threshold setting is much higher, in most cases greater than half the received signal level. In contrast to the noiseless channel, where less than one photon per information bit is required to produce decoded error probabilties on the order of 10^{-9}, we find that even when a high quality receiver ($Z = 1500$) is used, 20 to 40 received photons per information bit are required to produce these same error rates. When side information from the demodulator is available, the performance is about 1 dB better for overall error rates ranging from 10^{-7} *to* 10^{-11} and when $4 \leq L \leq 14$. It turns out that the performance is *exeedingly* sensitive to the threshold setting. This last result suggests that in situations where the signal level fluctuates considerably, an alternate demodulation strategy (e.g. δ_{max} or Maximum Likelihood Decoding (MLD)) may be required. An error probability comparison is made between "threshold" demodulation and MLD to access the penalty paid for using the simpler, but sub-optimum receiver.

Finally, we point out that as L increases, the capacity of the channel increases but approaches a finite limit in contrast to the noiseless channel that has infinite capacity as L increases without bound. In addition, as the PPM alphabet size increases, more bandwidth is required and the overall performance becomes even more sensitive to the threshold setting. This suggests that a moderate value for the alphabet size may be more advantageous when both complexity and sensitivity to signal levels are taken into account.

Spirulina: Cultures in Shaken vs. Stable Media

Ray A. Hill

Morgan State University
Associate Professor of Biology

The on-going challenge of the CELSS (controlled environmental life support system) group is to develop a reliable, functional controlled chamber in which edible plants can be grown aboard the spacecraft during long missions, minimizing the initial payload weight, and maximixing the use of re-cyclable materials aboard the spacecraft. CO_2, for example, can be utilized by select plants for conversion into edible, organic matter, and O_2, on the other hand a by-product of the process, can be utilized by persons aboard the spacecraft for necessary aerobic, metabolic functions. Several plants have been studied in detail under controlled chamber conditions to establish a data base on conditions necessary for maximum biomass yields, as well as control mechanisms for potentially harmful microorganisms that may represent endogenous contaminants on the seeds and/or seedlings used to initiate germination or planting (Dudzinski, Schwartzkopf). *Spirulina*, a filamentous member of the cyanobacterial population, has received increased interest by the CELSS group at NASA as a candidate organism for growth in a controlled environment. This interest stems, in part, from the comprehensive report on the edible qualities of *Spirulina* (Ciferri, 1983), high protein content a chief factor.

Becker (1978) reported the following nutritive value data of *S. platensis*:

Protein Efficiency	Net Protein Utilization	Biological Value	Digestibity Coefficient
1.80	62.0	75.0	83.0

Several studies confirm that persons living in several geographic areas have consumed *Spirulina* for food for many years (Pirie, 1975; Delpeuch, F., A. Joseph, and C. Cavelier, 1976). Protein content reports of *Spirulina* grown under laboratory conditions have ranged from 62 to 68% of dry weight (Clement, G., C. Giddey, and R. Menzi, 1967).

Current interests in laboratory culture of *Spirulina* involves the matting that forms as a result of the filaments intertwining during growth. Such matting possibly interferes with growth rates, i. e., minimizing protein yield, and quantitive research analyses. Dr. Ellen Weaver, San Jose State University has developed a defined growth medium for *Spirulina*, one that would minimize the matting as a result of intertwining. Dr. Richard Radmer of Martin-Marietta has also developed a defined medium to reduce mat formation during culture. Using the medium of Radmer at 37 °C, *Spirulina* was cultured under continuous flourescent light for 5 days. One inoculum was stable, while the other was shaken continuously. This was done to determine if continuous motion would reduce or inhibit mat formation as well as formation of previoulsly reported spiral and helical filaments. CO_2 was bubbled into both culture flasks. Spectrophotometric analyses showed that stable and shaken cultures grew at the same rate, however, mat formation was observed in the stable cultures. Microscopic examination of the cultures revealed that more filamentous spirals formed in the stable cultures, whereby straight filaments formed more prominently in the shaken cultures. The defined medium

seemed to reduce matting, however, the effect was more noticeable in the shaken cultures. The mechanism for reducing matting by using a defined medium is thought to be related to salt content. Further studies are at hand to determine the relationship of salt content to helical filament formation and spiral filament formation as compared to straight filament formation. The stage is also set for futther studies on Spirulina to more accurately determine protein content and identify amino acid composition.

REFERENCES

Becker, E. W. 1978. The legislative background for utilization of microalgae and other algal types of single cell protein. Arch. Hydrobiol. 11: 56-64.

Ciferri, Orio. 1983. Spirulina, The Edible Microorganism. Microbiological Reviews (47:4) pp.551578.

Celment, G. C. Giddey, and R. Menzi. 1967. Amino acid composition and nutritive value of the alga Spirulina maxima. J. Sci Food Agric. 18: 497-501.

Dudzinski, D., and S. Schwartzkopf. 1983. (personal communication).

Pirie, N. W. 1975. The Spirulina algae. pp. 33-34. In N.W. Pirie (ed.), Food Protein Sources. Cambridge University Press.

GROWTH RATE OF SPIRULINA
[OPTICAL DENSITY]

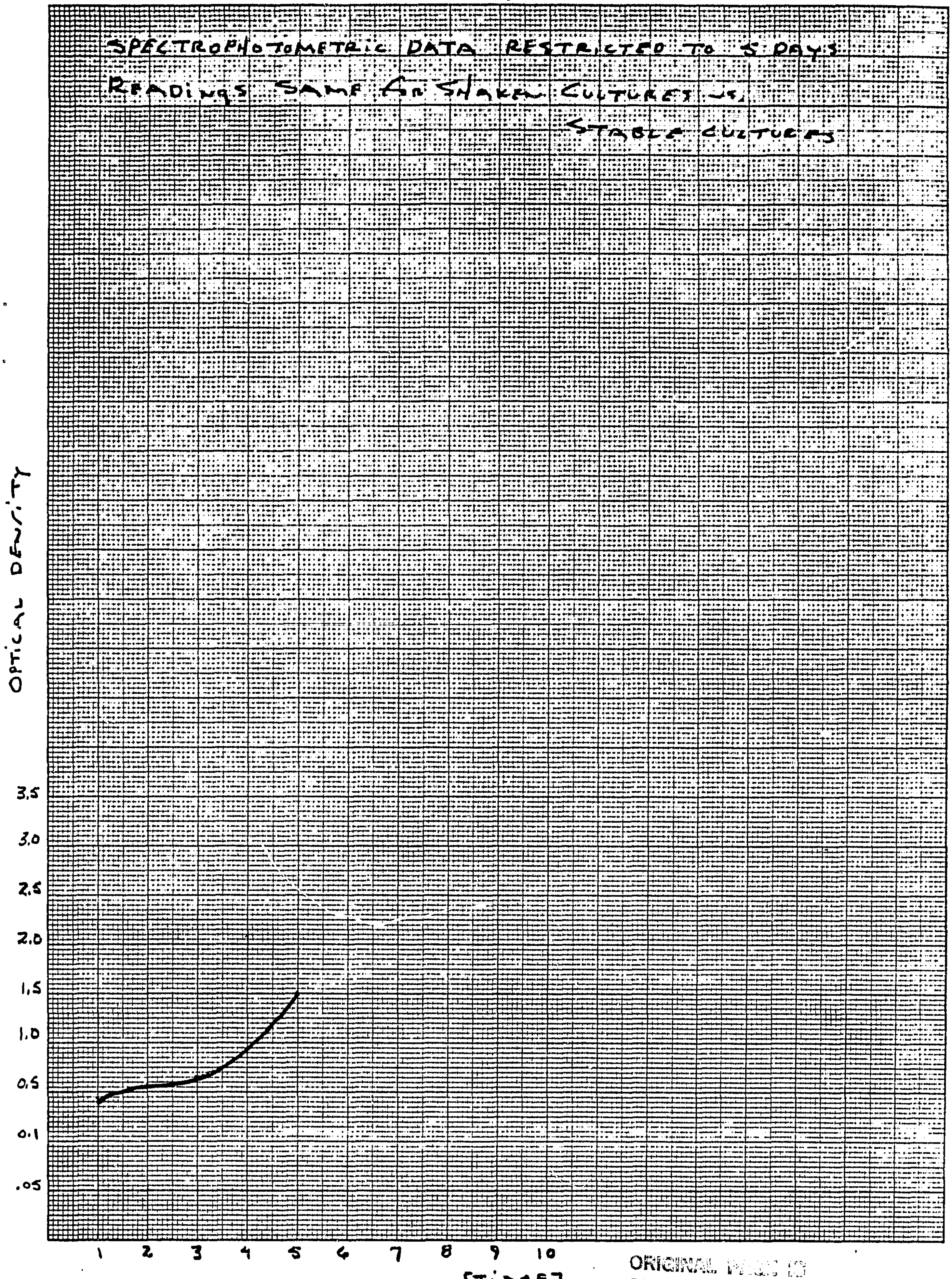

K+E 10 X 10 TO THE CENTIMETER 18 X 25 CM. KEUFFEL & ESSER CO. 46 1510 MADE IN U.S.A.

ORIGINAL PAGE IS
OF POOR QUALITY

Separated Flows Near the Nose of a Body of Revolution

Sung P. Lin

Clarkson University

The first project is on the flow separation from a deforming circular cylinder. This problem arises in an effort to understand how three-dimensional flow separation takes place near the nose of a body of revolution making an angle of attack with a uniform stream[1]. To obtain an analytical solution to this problem, an iterative method of solving the unsteady Navier-Stokes equation was invented last summer. The method involved, in the last step, solutions of some integral equations which were singular. A mean is now found to eliminate the singularities. To check the accuracy of the method and computation we have determined the time history of the migration of primary separation points on a rigid circular cylinder. The results are compared with known numerical and experimental results. The comparison is very good as can be seen in Fig. 1. The next step is to obtain the separation points on a deforming cylinder. This will be followed by the mapping of the unsteady separated flow fields. We hope to complete this project by the end of next year.

The second project is on the formation of spiral vorticies on a rotating body of revolution with a nose tip. The onset of vortical flows at some distance downstream from the nose is considered as the consequence of the instability of the axisymmetric basic flow about the rotating body. The basic flow varies rapidly in space. As a consequence, no known stability theories are adequate for our purpose of predicting the onset of the spiral vorticies. A new approach of stability analysis of non-parallel flows is formulated. An important realization is that the non-parallel flow instability can be solved completely only if it is treated as an initial value problem. The basic steady flow is currently being obtained by use of the Galerkin method. The general method is being used to generate known solutions of flows about a rotating sphere at small Reynolds numbers and over a disk rotating at large Reynolds numbers. This part of the work is expected to be completed by the end of this year. The basic flows about a cone and other bodies of revolution and their stability analysis will be carried out next year.

Other related projects I have initiated during my stay at Ames this summer include the formulation of stability analysis for the flows near saddle points of separation,[2] and the reinterpretation of three dimensional steady separation[3] in the frame work of dynamical systems.

Without the close interaction with Murray Tobak and the encouragement and support of Gary Chapman and Lewis Schiff, whatever progress I have made would not have been possible. All of the projects I studied at NASA-Ames are relevant to the mathematical modeling of the aerodynamic characteristics in flight dynamics.[3,4]

References

1. Peake, D.J. and Tobak, M., "On Issues Concerning Flow Separation and Vortical Flows in Three Dimensions", NASA TM 84374, 1983.

2. Kovasgnay, L.S.G., "Laminar Flow Behind a Two-Dimensional Grid", Proc. Comb. Phil. Soc. 44, 56-62, 1948.

3. Tobak. M. & Peak, D.J., "Topology of Three-Dimensional Separated Flows", Ann. Rev. Fluid Mech. 14, 61-85.

4. Tobak, M., Chapman, C.T., & Schiff, Lewis, B., "Mathematical Modeling of the Aerodynamic Characteristics in Flight Dynamics", NASA TM 85880, 1984

OF POOR QUALITY

IMPULSIVELY STARTED.

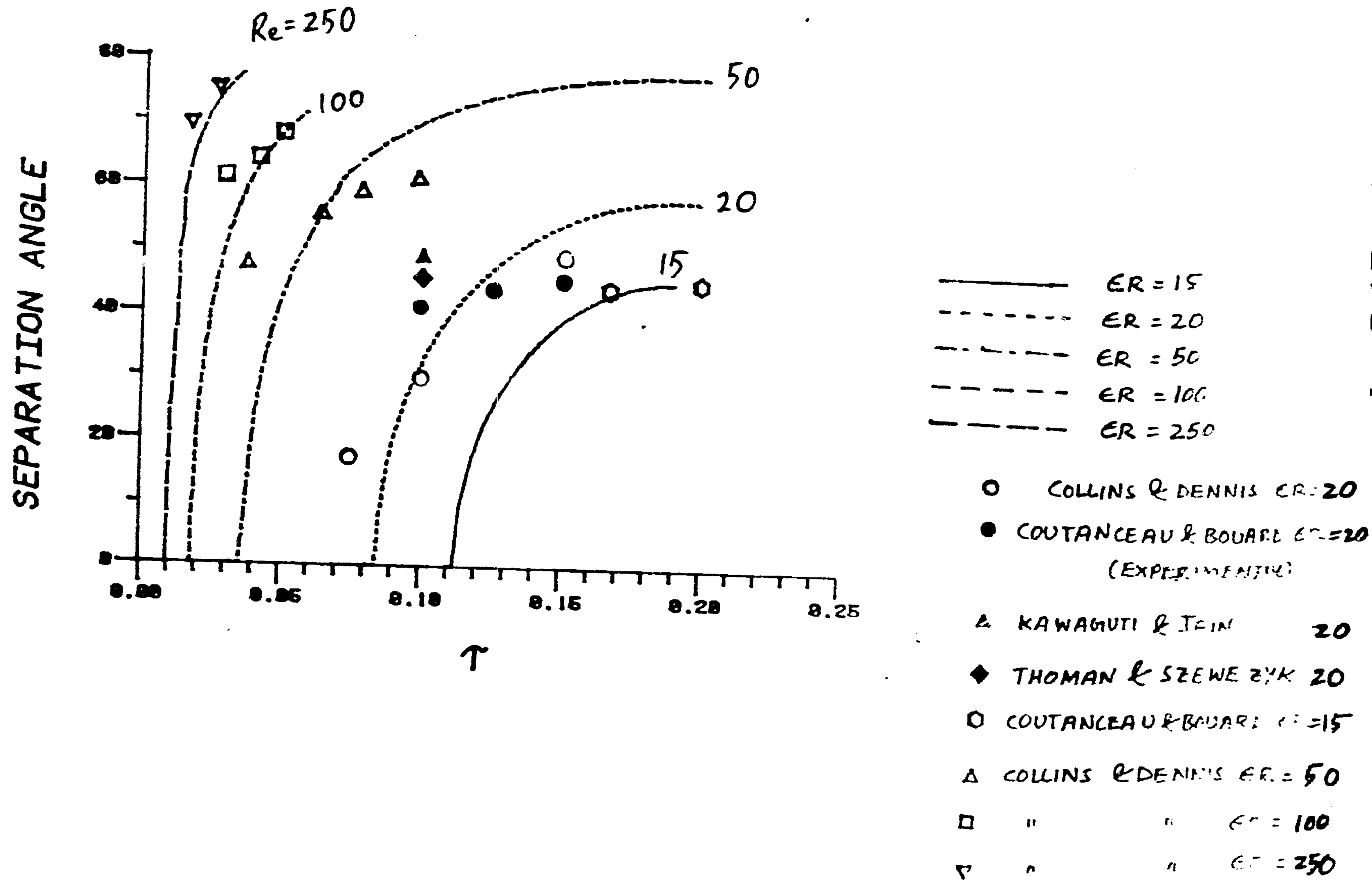

A Cross-Validation of a Logistic Regression Model for Predicting Tolerence During $+3G_z$ Acceleration

David A. Ludwig

University of North Carolina at Greensboro

Assistant Professor of Mathematics

Results of the analysis from last years investigation at NASA Ames indicated that after bedrest various physiological and demographic variables could not be used to predict how long human subjects could tolerate $+3G_z$ acceleration. The only variable which could be used to predict $+3G_z$ tolerance after bedrest was pre bedrest $+3G_z$ tolerance time. The question was then asked if pre bedrest tolerance could be predicted using the same independent variables. The analysis indicated that pre bedrest tolerance time could be predicted with very little error. The variables with the best predictive power included age, sex, and height. An older, shorter male was found to be a beneficial profile for increased tolerance time. Variables with moderate predictive power included weight (heavier subjects have higher tolerance), diastolic blood pressure (higher pressure was beneficial), and plasma volume per kilogram of body weight (less volume was beneficial). Variables that had no predictive power were those related to measures of fitness (VO_2 max, resting heartrate, and percent body fat). This result for the fitness variables was probably the most significant finding since it has not yet been agreed upon as to whether increased fitness is beneficial or detrimental to $+3G_z$ tolerance. Apparently other variables are much more important than fitness and leave little variance for fitness variables to explain. Subjects used to create the model could be correctly classified into high and low tolerance groups with 90 percent accuracy.

The value of this prediction model needs to stand up under cross-validation before its true worth is known. Using 16 new subjects who participated in the bedrest study for 1984 the model derived in 1983 was subjected to cross-validation. Results indicated almost as good a prediction under cross-validation as with the original data that derived the model. The original model predicted low and high tolerance groups for the 16 new subjects with 85 percent accuracy. The reduction of 5 percent is minimal and indicates that the original results from last year seem to be very reliable. Additional subjects with varying profiles across the independent variables need to be tested before the final predictive power of the current model is determined.

Although my main activity within the Biomedical Research Division was to determine the parameters for a model to predict $+3G_z$ tolerance, I also consulted with a variety of researchers within the division. I provided statistical consultation for the design and analysis for current studies and studies to be proposed in the future. I advised programmers who were writing statistical programs to be used within the division and helped interpret results from statistical packages currently running at Ames.

An Estimate of Aerosol Effects on the Inference of SO_2 Concentration in the El Chichon Volcanic Plume

J. L. Mergenthaler

Assistant Professor of Meteorology

Florida State University

There were no in-situ and few remote measurements of the composition of the stratospheric cloud resulting from the March 28 through April 4, 1982 eruptions of El Chichon during the first few days of its existence. Satellite observations of the atmosphere's spectral reflectivity gathered with the total ozone mapping spectrometer(TOMS) aboard Nimbus 7 were used by Krueger(1983) to infer the SO_2 mass in the stratospheric plume on April 6 after the major eruptions of April 3 and 4. The accuracy of this estimate, 3.3 megatons, is of great interest since it sets the initial conditions for the evolution of the sulfuric acid aerosol later observed.

A possibly important aspect of this measurement not treated by Krueger is the effect of the volcanic ash and other aerosol embedded in the plume. The neglect of these particulates could result in erroneous SO_2 amounts.

Figure 1 is a slightly adapted version of Figure 2 from Krueger's report. It depicts a spectral scan for five wavelength channels of the area perturbed by the stratospheric volcanic plume. An example is presented by Krueger in which this data is used to retrieve the columnar SO_2 concentration in part of the April 5 plume, scan 92. This example is reexamined taking into account the effects of aerosol scattering and absorption upon the plume albedo with the purpose of examining the magnitude of the error in stratospheric SO_2 mass previously reported and to examine limitations on the aerosol optical properties consistant with the measurements shown in Figure 1.

A three layer radiative transfer model has been developed to represent the reflectivity of the atmosphere containing a volcanically perturbed strata between 44 and 22mb. In the unperturbed case only the scattering from air and ozone absorption need be considered above 44mb. The reflectivity of the atmosphere below 44 mb is assumed to be Lambertian and is computed from the off-plume part of the scans shown in Figure 1. In computing the reflectivity of this layer the climatological ozone amount has been used to adjust for the attenuation caused by the ozone above 44mb. The volcanically perturbed stratum is assumed to contain aerosol and SO_2, as well as, ozone and air. The reflectivity of this layer and the underlying reflector is computed with a matrix-method doubling-adding radiative transfer code similar to that developed by Twomey, Jacobowitz and Howell (1966).

It has been assumed that the reflected radiance which would have been measured had the plume not intervened can be approximated by interpolating the spectral reflectivity data across the disturbed area as indicated by the dashed lines in Figure 1. It is pretty clear that the reflectivity at 312.5 and 317.5nm was reduced substantially by the plume; however, the reflectivity at 380.0nm appers to have been enhanced slightly, approximately 4% figuring by the procedure outlined above.

A phase function computed through the use of Mie theory with an asymmetry factor of .83 was used to represent the scattering pattern of rather large particles in the volcanically perturbed stratum. The single scattering albedo and optical depth of the aerosol are considered dependent variables to be determined from the observed reflectivities at 339.8, 331.2 and 380.0nm.

Model results shown in Figure 2 demonstrate that the reflectivity of the atmosphere at 339.8nm is very sensitive to aerosol scattering. Figure 2 shows for example that a model aerosol optical depth of 1.0 of conservatively scattering aerosol would have brightened the perturbed atmosphere by a few percent, and increase which would be easy to detect. Similarly, a unit optical depth of an aerosol with single scattering albedo .95 would have caused a decrease larger than any changes observable in the Figure 1 data. If an aerosol with a single scattering albedo very close to .984 was present, the reflectivity of the plume would be very nearly independent of optical depth. So a wide range of optical depth of this model aerosol would match the reflectivity observations of the plume at 339.8 and,due to their similarity,331.2nm. That is, the difference caused by the plume was very small.

Figure 2 also depicts the effect of aerosol on the reflectivity of the perturbed atmosphere at 380.0nm The maximum aerosol optical depth consistant with the 339.8 and 380.0nm data is about 1.50 where the aerosol has a single scattering albedo of about .984. Aerosol of this optical depth with a different single scattering albedo would change the reflectivity at 339.8 nm in a manner not observed. On the otherhand, given this single scattering albedo, the aerosol optical depth is limited by the observed increase in the albedo at 380.0nm.

The effect of aerosol upon the reflectivity at the shorter wavelengths which are strongly absorbed by SO_2 is now examined. The reflectivity of the model perturbed atmosphere is computed using Krueger's estimates of 67matm-cm to compute the reflectivity at 317.5nm and 61matm-cm to compute the model reflectivity at 312.5nm with no aerosol present. Different amounts of SO_2 were needed to explain the observed reflectivity for the 339.8-317.5nm and 331.2-312.5nm pairs. This discrepancy has been attributed primarily to uncertainties in SO_2 absorption coefficients. When the model aerosol described above is added keeping Krueger's estimated amounts of SO_2 for each of the short wavelength reflectivity computation, the reflectivity is observed to decrease in both cases as shown in Figure 3. By decreasing the amount of SO_2 from 67 to 59.5 matm-cm and from 61 to 59.5matm-cm the reflectivities computed at 317.5 and 312.5nm, respectively, can be matched with a volcanically perturbed stratum which is consistant in its properties for all wavelengths. This layer would contain 59.5matm-cm of SO_2, and a model aerosol with an optical depth of 1.5, a single scattering albedo of .984, and an asymmetry factor of .83.

The primary result of this work is a demonstration that the errors introduced into Krueger's TOMS inference of SO_2 amountare in the nieghborhood of 10% or less and not a factor of 3 or 4 which one might expect in light of other investigations which dealt with measurements of,or indirect inferences of,the amount of stratospheric SO_2 observed after the El Chichon eruption.(see Capone, et al.(1983) or Evans and Kerr(1983))

Another interesting result is that inconsistancies in measured SO_2 amount could result from aerosol effects; however, this does not rule out inaccuracies in SO_2 coefficicients as the source of inconsistancy in this case. The aerosol optical depth and single scattering albedo derived in this investigation are consistant with the observations of optical depth at Hawaii reported by Deluisi et al.(1983). They report an optical depth of about .75 at 425nm at that date, a time when the cloud was probably somewhat dispersed. This compares favorably with the maximum depth of 1.5 derived in this study for the April 5 case.

OF POOR

References

Capone, L.A.,O.B.Toon,R.C.Whitten,R.P.Turco,C.A.Riegel,and K.Santhanam, A Two-Dimensional Model Simulation of the El Chichon Volcanic Eruption Cloud, Geo. Res. Lett.,10,1053,1983.

Deluisi,J.J.,E.G.Dutton,K.L.Coulson,T.E.Defoor, and B.G.Mendonca, On Some Radiative Features of the El Chichon Volcanic Dust Cloud and a Cloud of Unknown Origin Observed at Mauna Loa, J. Geophys. Res.,88,6769,1983.

Evans,W.F.J.,and J.B.Kerr,Estimates of the Amount of Sulfur Dioxide Injected into the Stratosphere by the Explosive Volcanic Eruptions: El Chichon, Mystery Volcano, Mt. St. Helens, Geo. Res. Lett.,10,1049,1983.

Krueger,A.J.,Sighting of the El Chichon Sulfur Dioxide Clouds with the Nimbus 7 Total Ozone Mapping Spectrometer, Science,220,1377,1983.

Twomey,S.A., H.J.Jacobowitz,and H.B.Howell, Matrix Methods for Multiple Scattering Problems, J. Atmo. Sc.,23,289,1966.

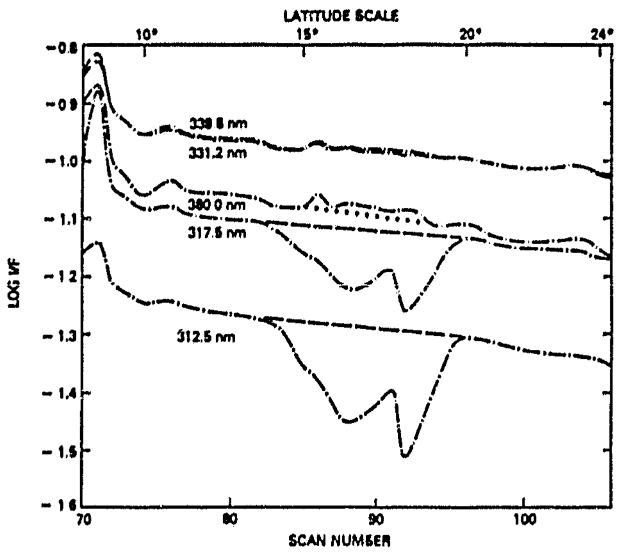

Figure 1. Effects of El Chichon cloud on TOMS reflectivities. Logarithm of spectral reflectivity along the same trace for five wavelengths. (Adapted from Krueger,1983) The dotted line interpolating the unperturbed reflectivity at 380nm was added by the author.

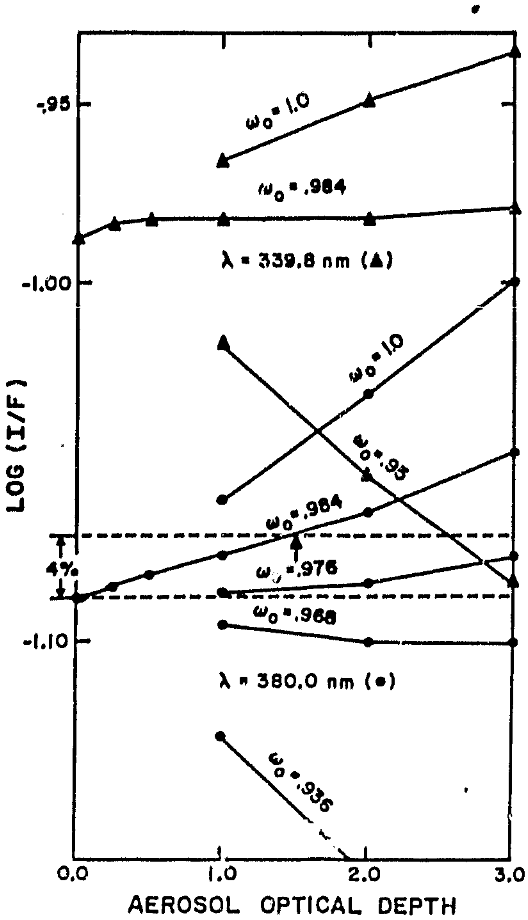

Figure 2. The effect of plume aerosol optical depth and single scattering albedo on computed atmospheric reflectivity at two TOMS wavelengths. The arrow indicates the aerosol optical depth at which a further increase in the aerosol loading would cause the computed aerosol loading to exceed the observed reflectivity increase at 380nm.

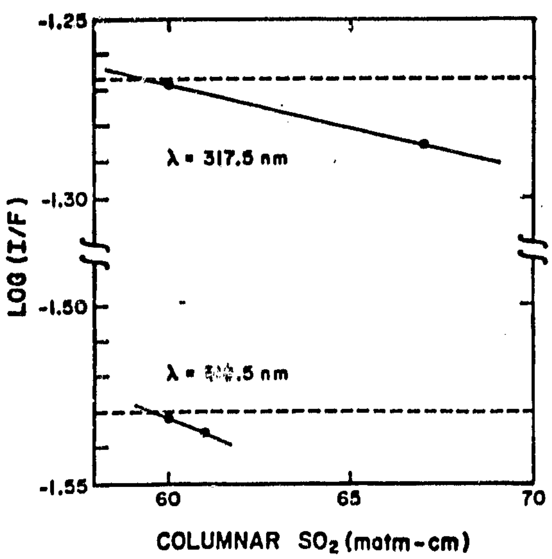

Figure 3. The dependence of atmospheric reflectivity on columnar SO_2. The plume layer is assumed to contain an optical depth of 1.5 of aerosol with a single scattering albedo of .984. Horizontal dashed lines show computed model reflectivities without aerosol at 312.5 and 317.5nm with 61 adn 67 matm-cm of SO_2, respectively. The plotted points show the effect of variations in columnar SO_2, when the model aerosol is present.

Nonlinear Analysis of the HiMAT Outer Wing

by Larry Nelson

Cal Poly State University
Professor, Mechanical Engineering

The HiMAT outer wing has, as the primary load carrying structure, aeroelastically tailored, laminated graphite/epoxy skins. Laminate coupon test data show that the wing has significant untapped load carrying potential. To utilize this potential requires, in part, that a nonlinear structural analysis be performed.

A preliminary, nonlinear analysis has been performed this summer. The basis for this analysis is an analytical representation of the experimental stress-strain behavior of the ply material--in this case Hercules AS/3501-5. The analytical representation is in the form of a Ramberg-Osgood fit (references 1 and 2) to the experimental data. The analytical curves are differentiated to give local tangent moduli, allowing the nonlinear problem to be replaced by a series of piece-wise linear problems, each of which may be solved by classical laminate plate theory, then appropriately added together to give an approximation of the nonlinear behavior of the laminate under load (Reference 3). Figure 1 compares the results of both a linear and nonlinear analysis with coupon test data acquired on the HiMAT laminate, $(50/-50/35/-50/50)_{2S}$. It is seen that the nonlinear analysis predicts quite well the coupon behavior. Based on the same failure criteria of maximum shear stress equal to 10 ksi, the nonlinear theory also better predicts laminate failure than does the linear theory.

The above described analysis can only be as good as the data base; i.e., the experimental stress-strain behavior of the individual plys. In the case of Figure 1, only the nonlinear ply shear behavior was estimated from (± 45) laminate data of Reference 4. It is believed that significant nonlinear ply behavior also exists in transverse compression. At the present time definitive, reasonably unambiguous stress-strain data for the ply material have not been located. A literature search continues.

The results of Figure 1 give confidence that a nonlinear analysis of a complex structure such as the HiMAT outer wing can be carried out. The basic approach will be to perform a series of piece-wise linear NASTRAN, incremental loads analyses, in which the stress-state of perhaps 100-150 locations in the composite wing skins will be monitored as progressively larger loads are (analytically) applied. The properties of the composite

material at each of these locations will be modified in accordance with the current stresses. It is anticipated that this effort will be continued by the writer upon his return to Cal Poly in a joint effort with Ames Dryden, Aerostructures Branch. It is foreseen that the HiMAT outer wing will be tested in the Ames Dryden Loads Test Facility, allowing a comparison between test and theory.

References

1. W. Ramberg and W.B. Osgood, "Description of Stress-Strain Curves by Three Parameters", NCA-TN-902, 1943.

2. Hashin, Z., Bagchi, D., and Rosen, B.W., "Non-linear Behavior of Fiber Composite Laminates", NASA CR-2313, 1974.

3. Pefit, P.H., and Waddoups, M.E., "A Method of Predicting the Nonlinear Behavior of Laminated Composites", J. Composite Mats., Vol. 3, pp. 2-19, January 1969.

4. Lagace, P.A., "Nonlinear Stress-strain Behavior of Graphite/Epoxy Laminates", Structures, Structural Dynamics and Materials Conference, 25th. Palm Springs, CA, May 14-16, 1984.

FIGURE 1. COMPARISON OF HIMAT COUPON TEST DATA WITH LINEAR AND NONLINEAR LAMINATE ANALYSIS THEORY

OF POOR

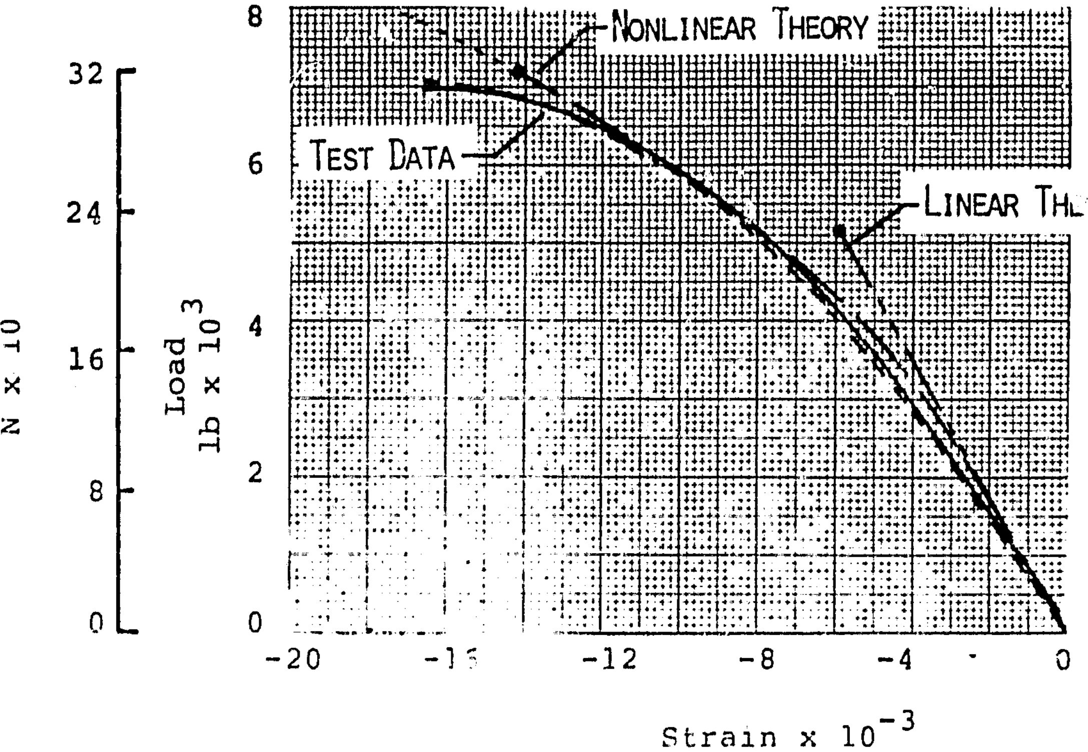

GAGE B

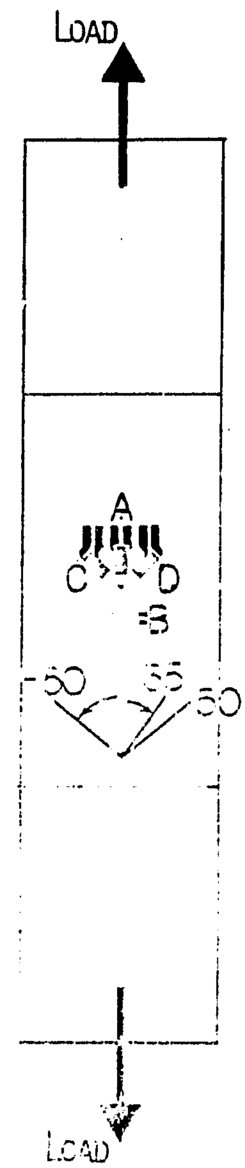

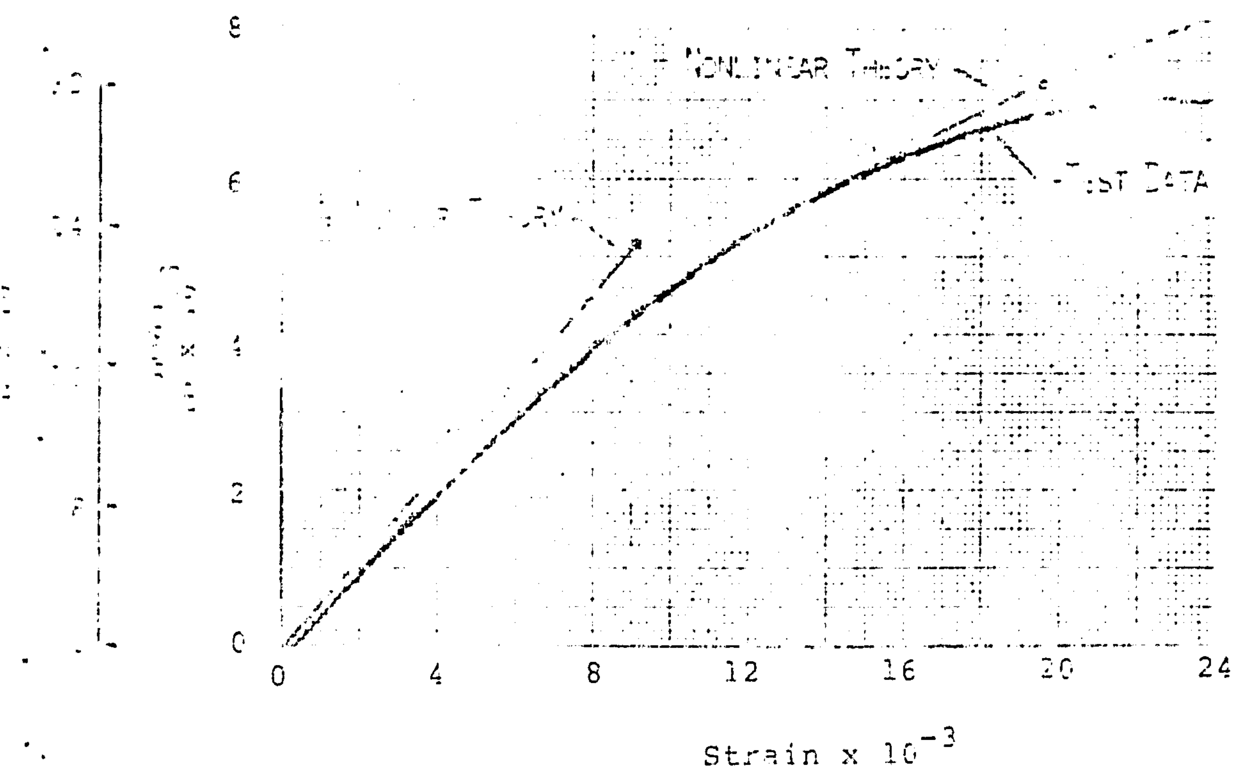

GAGE A

IN VIVO CHANGES IN NMR PARAMETERS OF RAT MUSCLE WITH EXERCISE

Felix S. Palubinskas, Ph.D., M.D.

10 August 1984

The object of the present investigation was to find out if measuring the NMR parameters (T1, T2, and H) of the fore limb and hind limb muscles of rats, in vivo, can tell us something about how these muscles respond to different exercise regimens. In particular, we wanted to find out if the suspended rat model, which appeared to simulate the condition of weightlessness for bone, would also simulate the condition of weightlessness for muscle.

A number of model systems have been used in an attempt to simulate weightlessness (1). The reasons for using land-based model systems are the following: they reduce the expense and difficulty of performing experiments, and they increase the frequency and convenience of experimentation.

The Soviets have found that muscle atrophy occurs in rats in space flight and in ground-based, immobilized rats (2,3). Americans have found that the changes found in bone in a suspended rat model appear to simulate those found in space flight (4).

MATERIALS AND METHODS

In our experiment we studied three sets of rats by proton NMR:

(1) rats whose hind limbs were <u>suspended</u>,

(2) <u>control</u> rats, and

(3) rats run in exercise cages (we called these rats <u>runners</u>).

By including the set of runners, we widened our investigation beyond that of just the determination of the effect of hind limb suspension to include the effect of exercise history.

The explanation of the details of how an NMR image is obtained using only radio waves incident on an animal placed in a strong magnetic field is given in Davis et al (5), and will not be

discussed here. Suffice it to say that this is an established technique for obtaining images and NMR parameter values of a human or animal body without using x-rays, or any invasive procedure, and without harming the animal in any way. The benefits of this technique are substantial, as the animal subject can be followed serially, in subsequent or sequential studies, with the prospect of using the subject as its own control.

The experiment was run for 13 days at Ames. Three sets of rats were individually caged: four controls, four suspended rats, and five runners. Two rats from each of the three sets were selected for imaging. The initial weights of these rats ranged from 138 to 156 grams. After the second day of the experiment, the rats gained weight almost linearly, ending up with weights that ranged from 210 to 257 grams on the 13th day. Suspended rats ended up heavier than the controls which in turn ended up heavier than the runners.

After completing thirteen days in the experiment, the rats were transported from Ames to the Radiation Imaging Laboratory of UCSF at Oyster Point and imaged.

It took about an hour to image each rat. For each body region imaged, a five-slice sequence was taken using two repetition times (0.5 and 1.0 sec) for each of which two spin echos were recorded (at 28 and 56 millisec). Four averages were made for each of the four possible conditions. Subsequently, each of the images was called up on the computer and a region of interest enclosed using a trakball. The computer then automatically computed the NMR parameters.

RESULTS

The NMR data were plotted in the T1-T2, T1-H, and T2-H planes. When the data were so mapped, any differences that existed between the corresponding muscle regions of the three sets of rats showed up clearly. In addition, the NMR values for the fore limb and hind limb muscles of each individual rat could be compared, permitting the rat to serve as its own control.

Examination of the maps showed:

<u>In the T1-T2 plane</u>:

(a) The hind limb muscles of <u>suspended</u> rats clearly map in a different region of the plane than the hind limb muscles of <u>controls</u> and <u>runners</u>.

(b) The fore limb muscles of <u>suspended</u> and <u>control</u> rats map roughly in the same part of the plane, whereas the fore limb muscles of <u>runners</u> map in a distinctly different part of the plane.

<u>In the T1-H plane</u>:

(a) The hind limb muscles of <u>suspended</u>, <u>control</u>, and <u>runner</u> rats map in widely separated regions of the plane.

(b) The fore limb muscles of <u>suspended</u> and <u>control</u> rats map in roughly the same region of the plane, whereas those of the <u>runners</u> map in a widely separated region of the plane.

(c) The fore limb muscles of <u>controls</u>, and particularly the <u>runners</u>, map in substantially different regions of the plane than their corresponding hind limb muscles. The differences for the fore limb and hind limb muscles of <u>suspended</u> rats are slight.

<u>In the T2-H plane</u>:

(a) The fore limb muscles of all three sets of rats map in different regions of the plane than their corresponding hind limb muscles.

(b) The forelimb muscles of <u>runners</u> map in a substantially different part of the plane from those of <u>controls</u> and <u>suspended</u> rats.

<u>DISCUSSION</u>

What does all this mean?

It means that the exercise state of rats is reflected by their NMR parameters. Yet, although the measurements of NMR parameters are quantitative measures of the behavior of the so-called mobile protons in the plane of the tissue imaged, it is not at all clear today what precisely this means in terms of the molecular structure of the tissue. Nevertheless, it is our impression that by following the change of the NMR parameters of the muscles of an individual animal, the exercise state of various muscle groups, their development, or their state of

"exercise fitness" can be measured quantitatively, in vivo, and with complete safety.

To establish that the suspended rat model provides, for muscles, a satisfactory analog of the conditions of weightlessness in space flight will require NMR experiments involving space flight. Toward that end, an Intention To Propose document has been submitted to NASA Headquarters for such experimentation. In addition, a paper describing the present investigation is now being prepared and will be submitted for publication.

REFERENCES

(1) MOREY-HOLTON, E., and T.J. WRONSKI, Animal models for simulating weightlessness. The Physiologist 24: S-45-S47(1981).

(2) PORTUGALOV, V.V., E.I. ILYINA-KAKUEVA, V.I. STAROSTIN, K.D. ROKHLENKO, AND Z.F. SAVIK, Morphological and cytochemical studies of hypokinetic effects. Aviat. Space Environ. Med 42:1041-1049 (1971).

(3) ILYINA-KAKUEVA, E.I., V.V. PORTUGALOV, AND N.P. KRIVENKOVA, Spaceflight effects on the skeletal muscles of rats. Aviat. Space Environ. Med. 47:700-703 (1976).

(4) WRONSKI, T.J., AND E.R. MOREY, Effect of spaceflight on periosteal bone formation in rats. Am. J. Physiol. 244:R305-309 (1983).

(5) DAVIS, P.L, L. KAUFMAN, L.E. CROOKS, AND T.R. MILLER, Detectability of Hepatomas in rat livers by nuclear magnetic resonance imaging. Invest. Radiol. 16:354-359 (1981).

^{3}He Refrigeration for Space Applications

Andres F. Rodriguez

Professor, Physics Department
University of the Pacific
Stockton, CA 95211

The low temperature provided by ^{3}He refrigerators (0.3 - 3^{o}K) have useful space applications. However, while ^{3}He refrigeration has been used on Earth for a number of years and in aircraft and spin-stabilized rockets, it has yet to be used in the low gravity environment of space.

The low temperature and the low surface tension of ^{3}He require special design considerations for a space-compatible ^{3}He refrigerator. These considerations include:

a) The need for small pores in a metal matrix to condense ^{3}He vapor and to contain the liquid (capillary confinement).

b) The effects of bubble nucleation and growth.

c) The effects of the thermal conductivity within the matrix.

These design considerations, along with a possible confinement system have been studies since last summer by this fellow and his NASA-Ames colleague Dr. Peter Kittel.

During last summer, work was done on the validity of the model of the porous metal matrix proposed by Robertson et al. Also, the investigations of Ostermeier and his group on capillary confinement of cryogens in a metal matrix were used as the basis for this research project. The details of this work were included in the 1983 Summer Report.

As an outgrowth of the first year summer NASA-Stanford Program, this fellow received a NASA-Ames Consortium Agreement Grant. This grant provided support for the fellow to continue his work at Ames (September - December 1983) with Peter Kittel while being on sabatical from the home institution.

The work on design considerations for a ^{3}He refrigerator for space applications was continued at the house institution during the spring of 1984 with frequent trips to Ames for consultation and finished during this summer.

It has been concluded that it is feasible to design a ^{3}He refrigerator that will operate in the low gravity environment of space where accelerations can occur in random directions. The key to the design is to fill the liquid chamber with a high-conductivity porous material such as sintered copper. The pores allow surface tension forces to contain the liquid while the conductivity ensures that the evaporation occurs at the surface of the matrix rather than internally. The matrix also provides a favorable place for condensation to occur and suppresses bubble nucleation and movement.

This research project includes mathematical and physical analysis of the role and strength of surface tension forces, use of the Marangoni Effect, effect of lateral accelerations described in terms of the Bond number and prevention of bubble nucleation and motion of bubbles. Finally, a discussion on how these considerations can be applied to the design of a refrigerator are included. One paper was presented at the National Conference of the ASEE and published in the Proceedings (3, 1332-1334, 1984). In addition, a technical memo was published by NASA (TM-85973, 1984) and a paper is being prepared for publication.

Dr. Kittel is attending an international conference in Berlin where he will present some of our results.

Additional work is being done this summer on the pumping speed of cryogens through the pores of a matrix. Also, we are addressing other problems related to the surface tension of ^{3}He - ^{4}He mixtures and the presence of surface levels in solutions of ^{3}He in ^{4}He.

A detailed treatment of our work could be found in:

1) Rodriguez, Andres F., "Capillary Confinement of Cryogens in a Porous Metal Matrix", Proceedings 1984 Annual Conference ASEE, 3, 1332-1334, (1984).

2) Kittel, Peter and Rodriguez, Andres F., "Design Considerations for a ^{3}He Refrigerator for Space Applications", NASA TM-85973 (1984).

From a professional point of view, this program has been very rewarding for this fellow both for the research work that will be continued and for the impact that it will have in my teaching performance.

REFERENCES

1. Kittel, P.: Refrigeration Below 1 K in Space. Physica, vol. 108B, Aug. 1981, pp. 1115-1118.

2. Kittel, P.: Sub-Kelvin Temperatures in Space. Adv. Cryo. Eng., vol. 27, 1982, pp. 745-749.

3. Chanin, G.; and Torre, J. P.: A Portable ^{3}He Cryostat for Space Applications. Proc. Sixth Int. Cryo. Eng. Conf., IPC Science and Technology Press, 1977, pp. 96-98.

4. Kittel, P.; and Brooks, W. F.: Demountable Self-contained ^{3}He Refrigerator. Adv. Cryo. Eng., vol. 27, 1982, pp. 727-734.

5. Woody, D. P.; and Richards, P. L.: Spectrum of the Cosmic Background Radiation. Phys. Rev. Lett., vol. 42, Apr. 1979, pp. 925-929.

6. Radostitz, J. V.; Nolt, I. G.; Kittel, P.; and Donnelly, R. J.: Portable ^{3}He Detector Cryostat for the Far Infrared. Rev. Sci. Instrum., vol. 49, Jan. 1978, pp. 86-88.

7. Gush, H.: Rocket Measurement of the Cosmic Background Submillimeter Spectrum. Proc. Space Helium Dewar Conference (to be published, U. of Alabama Press, 1984).

8. Urbach, A. R.; and Mason, P. V.: IRAS Cryogenic System Flight Performance Report. Adv. Cryo. Eng., vol. 29, 1984, pp. 651-660.

9. Ostermeier, R. M.; Nolt, I. G.; and Radostitz, J. V.: Capillary Confinement of Cryogens for Refrigeration and Liquid Control in Space — I. Theory. Cryogenics, vol. 18, Feb. 1978, pp. 83-86.

10. Ennis, D. J.; Kittel, P.; Brooks, W. A.; Miller, A.; and Spivak, A. L.: A ^{3}He Refrigerator Employing Capillary Confinement of Liquid Cryogen. Refrigeration for Cryogenic Sensors, NASA CP-2287, 1983, pp. 405-417.

11. Donnelly, R. J.; Kittel, P.; Ostermeier, R. M.; Radostitz, J. V.; Lee, B. R.; and Cooper, J. C.: A Study of Confinement and Heat Transfer Properties of Cryogens, Final Report, NASA Grant NSG-2208, 1979.

12. Satterlee, H. M.; and Reynolds, W. C.: The Dynamics of the Free Surface in Cylindrical Containers Under Strong Capillary and Weak Gravity Conditions." Report LG-2, Mechanical Engineering Dept., Stanford University, 1964.

13. Alexander, G. E.; Barksdale, T. R.; Hise, R. E.; Lunden, K. C.; and Paynter, H. L.: Experimental Investigations of Capillary Propellant Control Devices for Low Gravity Environments, vol. II, Final Report, NASA Contract NAS8-21259, Martin Marietta Corp., 1970.

14. Labuntzov, D.; Evdokimov, O. P.; Tishin, I. V., and Ul'ianov, A. F.: Analytical Investigation of the Boiling Process in Small Diameter Tubes. Mashinostroenie, vol. 7, 1970, pp. 68-73.

15. Smith, R. V.: The Influence of Surface Characteristics on the Boiling of Cryogenic Fluids. Trans. ASME. J. of Eng. for Indust., vol. 91, Nov. 1969, pp. 1217-1221.

16. Bald, W. B.: Bubble Nucleation at Real Surfaces with no Pre-existing Gaseous Phase, Dept. of Engineering Report N-75-29279, University of Oxford, 1975.

17. Kottowski, H. M.: The Mechanism of Nucleation, Superheating and Reducing Effects on the Activation Energy of Nucleation. Prog. Heat and Mass Transfer, vol. 7, 1973, pp. 299-324.

18. McGrew, J. L.; Rehm, T. L.; and Griskey, R. G.: The Effect of Temperature Induced Surface Tension Gradients on Bubble Mechanics. App. Sci. Res., vol. 29, June 1974, pp. 195-210.

19. Young, N. O.; Goldstein, J. S.; and Block, M. J.: The Motion of Bubbles in Vertical Temperature Gradient. J. Fluid Mech., vol. 6, Oct. 1959, pp. 350-356.

20. Reif, F.: Fundamentals of Statistical and Thermal Physics. McGraw-Hill, 1965, pp. 304-306.

21. Rodriguez, Andres F., "Capillary Confinement of Cryogens in a Porous Metal Matrix", Proceedings 1984 Annual Conference ASEE, 3, 1332 - 1334, (1984).

22. Kittel, Peter and Rodriguez, Andres F., "Design Considerations for a ^{3}He Refrigerator for Space Applications", NASA TM-85973 (1984).

Stability for Block Tridiagonal Matrices

MOLLY SCHEFFÉ
Boston University

The real motivation behind this work is to understand issues like speed of convergence for relaxation methods to solve the Euler equations of fluid dynamics. If spatial derivatives in these equations are approximated by centered differences, a matrix operator can result like

$$M = \begin{pmatrix} 0 & A_1 & 0 & & \\ -A_0 & 0 & A_2 & \ddots & \\ 0 & -A_1 & 0 & \ddots & \ddots \\ & & \ddots & \ddots & \ddots \end{pmatrix} \qquad A_i\text{'s} = \text{matrix blocks of size } b$$

. The basic problem is to understand the structure of the eigenvalues of M — for a stable problem, they should all lie along the imaginary axis. Work by my NASA colleague, Dennis Jesperson, has shown that even when the individual blocks A_i are well-behaved, the eigenvalues of M may wander from the imaginary axis (instability). Very little seems to be known about this problem, partly because it is hard to generalize scalar results to the matrix level.

Although originally I was looking at pure Dirichlet boundary conditions, it seems easier to get results for boundary conditions where there is a nonzero block in the lower righthand or upper lefthand corner. Liapunov theory can be used to study the stability of M which means, equivalently,

- no eigenvalues λ with $\mathrm{Re}\,\lambda > 0$: prevents unbounded growth
- given a positive definite P, the matrix Ricatti equation $M^*H + HM = -P$ has a positive definite solution H.

I. Results for 1-dimensional problems $\frac{\partial u}{\partial t} + \frac{\partial}{\partial x}(Au) = 0$

1. Scalar case (u is scalar, $A = a(x)$)

Here I have made use of analogies with the work of H.R. Schwartz (for references, see [1]). He showed that if a matrix is similar to his canonical form

$$W = \begin{pmatrix} 0 & 1 & & & & \\ -w_1 & 0 & 1 & & & \\ & -w_2 & 0 & 1 & & \\ & & & \ddots & & \\ & & & & 0 & 1 \\ & & & & -w_{m-1} & -w_m \end{pmatrix}$$

then the Ricatti eqn $W^*D + DW = \begin{pmatrix} 0 & & & \\ & 0 & & \\ & & \ddots & \\ & & & -2w_m^2 \end{pmatrix}$ has an easy explicit diagonal solution $D = \begin{pmatrix} w_1 w_2 \cdots w_m & & & \\ & w_2 w_3 \cdots w_m & & \\ & & \ddots & \\ & & & w_m \end{pmatrix}$. When the w's are all nonzero, W is stable $\Leftrightarrow$ all the w_i are positive.

I have corrected some mistakes in the literature about just which matrices are similar to W's. Since the matrix above is very close to a central difference matrix, I've been able to use analogous arguments to

- describe all possible stable nonzero boundary conditions at the upper lefthand and lower righthand corners (Also in the interior, if the coefficient $a(x)$ changes sign somewhere in the spatial interval)
- show that if the coefficient $a(x)$ changes sign, there must be an $a_i = 0$ for stability. Desideri et al, [2], could show sufficiency, but now this Liapunov theory shows the condition is also necessary. This is of interest because it's a simple model of transition from subsonic to supersonic flow, where the numerics are

I also have found some interesting tridiagonal solutions T to the Ricatti problems

$$W^* T_1 + T_1 W = -P_1$$
$$M^* T_2 + T_2 M = -P_2$$

2. General case (u = vector of size m)

Here I can find some Liapunov functions for the partial differential equation, when the space variable x is continuous, using boundary conditions. In the scalar case, the discrete solution in #1 above tends to the continuous one in #2 as the mesh $\Delta x \to 0$. But so far I haven't found discrete block generalizations that tend to these continuous ones for $m > 1$.

II. Two-dimensional problems $\frac{\partial u}{\partial t} + \frac{\partial}{\partial x}(Au) + \frac{\partial}{\partial y}(Bu) = 0$

1. Scalar case

Here I can show that if $a_i = a(x_i)$ obeys the rules on the preceding page and $b(x) > 0$, then the resulting central difference scheme is stable. I'm also looking for continuous Liapunov functions as in #2 above, i.e. for the partial differential equation rather than the central difference equation

I wish I had the time to have already done everything! You can see various results here, but they may not be the most general possible final answers yet.

Well — thanks for a great summer, everyone!

Regards,
Molly Scheffé

[1] S. Barnett + C. Storey, Matrix Methods in Stability Theory, Barnes + Noble, NY, 1970, esp. §3.4, 6.4

[2] J-A Desideri, J.L. Steger, J.C. Tannehil, On Improving the Iterative Convergence Properties of an Implicit Approximate-Factorization FD Algorithm NASA TM 78495 (1978)

Analytic Properties of Upwind Schemes for The Euler Equations

Charles W. Schelin

The Euler equations amount to a system of conservation laws that model the inviscid flow of a perfect fluid. Numerous iterative schemes have been devised to solve discretized versions of these equations. Upwind schemes offer stable solutions to the difference equations by separating various signal directions. These schemes are usually classified as either flux-splitting or flux-difference splitting, depending on the approach used to separate the signal directions.

A number of desirable properties for a flux-splitting scheme have been given by van Leer [3]. Among these properties is a degeneracy condition designed to resolve stationary shock structures in a manner similar to the flux-difference scheme of Osher [2]. Comparing these schemes I found both resolve the numerical Riemann problem:

$$u_j = u^L \quad \text{for} \quad j < j_0 ,$$
$$u_j = u^R \quad \text{for} \quad j > j_0 ,$$

where $u^L > \bar{u} > u^R$, $\bar{u}$ being a sonic point, by yielding $u_{j_0} = \bar{u}$.

Using ideas similar to those developed during my first summer in the ASEE program, I devised a nonlinear relaxation scheme for a first order discretization of the one-dimensional Euler equations using the van Leer splitting. At some future time I hope to generalize this scheme to second order discretizations in two dimensions and general coordinates.

Dennis Jespersen of NASA-Ames has shown that three of van Leer's properties; interpolation, degeneracy and differentiability, are inconsistent in general coordinates. A flux-splitting possessing these three properties exists if and only if the coordinates are orthogonal. Hoping to draw some conclusion about flux-difference schemes I examined the Osher scheme.

Flux-difference schemes depend on a numerical flux $f(u,v)$ as well as the physical flux $f(w)$. Harten, Lax and van Leer [1] use the form

$$f(u,v) = [f(u) + f(v) - d(u,v)]/2 ,$$

where $d(u,v)$ represents an absolute flux difference, to define the numerical flux. By splitting $d(u,v)$ into

$$d(u,v) = d^{+}(u,v) + d^{-}(u,v),$$

where

$$d^{+}(u,v) = f(v) - f(u,v)$$

and

$$d^{-}(u,v) = f(u) - f(u,v),$$

I was able to define the local splitting

$$f^{+}(v) = f(u^{*}) + d^{+}(u^{*},v)$$

$$f^{-}(v) = - d^{-}(u^{*},v)$$

for a sonic reference point u^{*}. Using this local splitting, I was able to show that the Osher scheme is differentiable at u^{*} if and only if the coordinates are orthogonal.

Other flux-difference schemes can be shown to be differentiable. Specifically, any scheme satisfying the Harten, Lax, van Leer upwind condition is differentiable.

Since certain schemes which are smooth in Cartesian coordinates lose this smoothness in general coordinates it seems necessary to reexamine the transformed coordinate approach to flow problems in general geometries. Perhaps metric variables and flow variables can be separated in a fashion that will allow schemes to retain desirable properties. I plan to study this question in the future.

References

1. Harten,A., Lax,P., van Leer, B., "On Upstream Differencing and Gudonov Type Schemes for Hyperbolic Conservation Laws", SIAM Review, v.25, no.1, 1983, pp. 35-61.

2. Osher, S. "Numerical Solution of Singular Perturbation Problems and Hyperbolic Systems of Conservation Laws", in North Holland Mathematical Studies, v.47, 1981.

3. van Leer,B., "Flux-Vector Splitting for The Euler Equations", in Eighth International Conference on Numerical Methods in Fluid Dynamics, Springer Lecture Notes in Physics, no.170, ed. E.Kruse, 1983.

August 17, 1984

Preliminary Abstract Report

Vestibular Research Facility (VRF) - Design, Control and Safety Analysis of the Vestibular Research Centrifuge and Linear Accelerator

William Stamets, Adjunct Professor
University of Wisconsin - Parkside, Kenosha, Wisconsin

As a second-year Faculty Fellow at Stanford/NASA-Ames, I performed the following space-related research assignments during the summer 1984:

1. Preliminary Safety and Hazard Analysis Report on Vestibular Research Facility (VRF).

2. Stress Analysis Review of Impact, Seismic and Dynamic Loading of Experimental Centrifuge.

3. Collected and reviewed 21 library references pertaining to hazards, reliability, safety, codes and standards for industrial facilities.

4. Provided design assistance for the Linear Sled Research Accelerator.

Copies of the above-mentioned reports will be available in about 1 week.

The Preliminary Safety and Hazard Analysis Report deals with the identification of hazards and postulated accidents at the new VRF, Building N-242 and sets forth means for minimizing effects. It analyzes standard industrial equipment (crane, pressure vessel - air receiver tank, electric controls, etc.) and special purpose machinery (centrifuge and linear accelerator). The report is required by the NASA/Ames Safety Department before the facility can be activated.

The Stress Analysis studies examine potential impact of loose parts flying from the centrifuge and injuring personnel and adjacent equipment. A seismic study is included, which considers earthquake damage in accordance with "Seismic and Wind Design Criteria" published by Lawrence Livermore Laboratories.

Annotated copies of pertinent sections of the 21 Codes and Standards references are to be provided with the Hazard Analysis Report. Attention is drawn to those portions of the references which particularly affect the VRF.

My student, Daniel M. Eggert of Kenosha, Wisconsin, is here under an NASA/Ames student grant which we arranged last December. He is working on the drive design for the Linear Accelerator Sled and as Principal Investigator, I am overseeing his work. We participated in a Poster Show Friday afternoon July 20th at the Ames Cafeteria where performance characteristics of an air-bearing for the sled was demonstrated. Of some twenty exhibits, eight were chosen to be shown at the Dryden Flight Research Facility and Dan flew down there August 9th.

During the summer, I attended and participated in the following educational activities given by Stanford:

Computer Science CS-104 - Programming in PASCAL
Mechanical Engineering ME-219 - Robotics and Computer Vision
Aero/Astro AA-2995 - Seminar in Review of Current Research (Thursday evenings) in Aeronautics, Astronautics & Life Sciences.

Along with these, I participated in the Monday/Wednesday noon-time Research Review sessions and gave a 20-minute presentation on my work program July 11th. Also, I attended all of the Friday noon ASEE Summer Faculty Seminars which described a wide variety of space-related engineering subjects. All of these will be helpful to me in giving a talk next Fall when I have been invited to speak before our local engineering society.

William Stamets, P.E.

cc:
R. Mah

Analysis of Aerosol Particles by Expert System

Scott A. Starks

University of Texas at Arlington
Associate Professor of Computer Science and Engineering

Investigations into the concentration levels of aerosol particles in the earth's upper atmosphere have been conducted at Ames Research Center for a number of years. In particular, much research has been focused upon the study of sulphuric acid particles. Collection of aerosol particle samples in the stratosphere is accomplished by use of the Ames Wire Impactor which is mounted beneath the wing of a NASA U2 research aircraft. Current methods being used for classifying, counting, sizing, and developing size distributions of the collected samples are very labor-intensive. As a consequence, investigation was begun last year by the author, under the NASA/ASEE Summer Faculty Fellowship Program, to determine the feasibility of automating the current method of aerosol particle analysis.

It was discovered that commercially available image processing systems did not provide enough capability to discriminate the collected aerosol particles from contaminants and blemishes on the sampling surface. As a result, an automated approach based upon artificial intelligence techniques was formulated by the author. Work on this automated begun during the summer of 1983. It was continued by the author during the Academic year 1983-1984 under the NASA/Ames University Consortium Agreement NCA-OR780-401.

A system diagram of the hardware used in the system is shown in Fig. 1. A description of the operation of the system is summarized in the following. First, a sample is mounted in the ISI SX-30 scanning electron microscope (SEM). The SEM operator then focuses the microscope on the area of the surface to be examined. The analog video output signal from the SEM is then passed through a TV-30 signal interface. The interface converts the signal to a standard NTSC video format. This standard signal is then digitized by means of a Quantex video digitizer. A single video frame is "grabbed" by the digitizer under the control of an HP 1000/2100 minicomputer. The frame is sampled and quantized by the digitizer to form a (512X512) digital representation of the image. The minicomputer archives the data onto magnetic tape. Approximately 150 images are stored on a single magnetic tape and are used in the analysis of a single experiment. Once all the images have been recorded the magnetic tape is downloaded onto a VAX 11/780 computer.

Resident on the VAX computer is an expert system developed under this fellowship program for the automatic analysis of the aerosol particles. This system is called APES. A data flow diagram of the software organization of the expert system is shown in Fig. 2. The front end of the expert system, consisting of the filtering module, the edge detection module, and the image segmentation module are written in the computer language, C. The expert system control module is written in the computer language, LISP. An expert system building tool called MRS was used in the

development of the rule based classifier. The final output from the system is a complete description of particle size information. A more detailed description of the APES hardware and software systems are presented in [1], [2].

The major advantages of the automated approach over that of manual inspection are many fold. First of all, analysis by expert system yields a large increase in the speed of reducing aerosol particle data. Secondly, automated system achieve appreciably higher levels of accuracy in counting and sizing of particles. Lastly, the extraction of shape information by computer yields a more accurate assessment of particle volume.

It has been the pleasure of this fellow to work closely with a number of distinguished individuals in the development of APES. This fellow wishes to express his debt of gratitude to Dr. Henry Lum, Ms. Libby Netland, and Ms. Mary Duffy for their support and assistance in the completion of this project.

References:

[1] Starks, S.A. and Netland, L., "Automated Analysis of Aerosol Particles by Means of an Expert System", Proceedings of the 3rd Phoenix Conference on Computers and Communications, Phoenix, Arizona, March 1984.

[2] Starks, S.A., Netland, L., and Elizandro, D.W., "Analysis of Aerosol Particles by Digital Image Processing Techniques", Proceedings of the 1984 ASEE Annual Conference, Salt Lake City, Utah, June 1984.

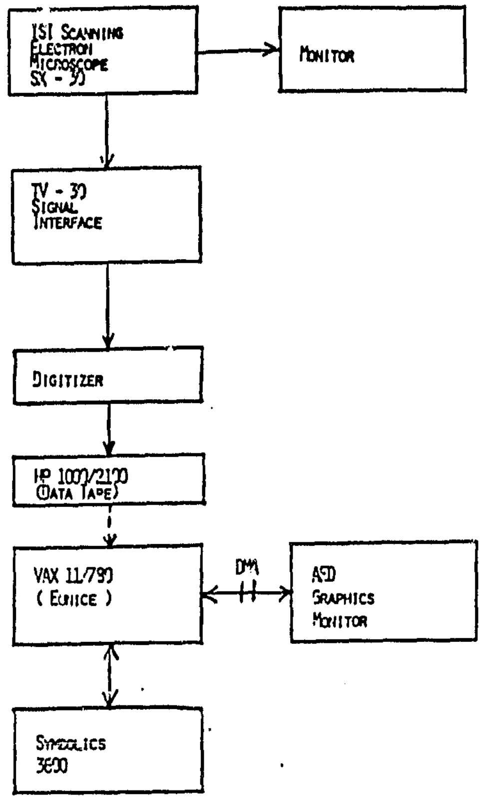

Figure 1. APES Hardware Configuration

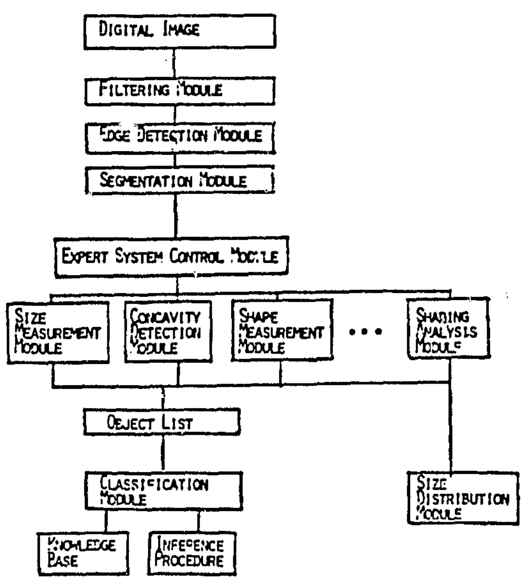

Figure 2. APES Data Flow Diagram